UNIVERSITY OF OKLAHOMA

GRADUATE COLLEGE

Time Dependent radiative Transfer: Applications on Core collapse Supernova and Cosmic recombination

A Dissertation

Submitted to the Graduate Faculty

in partial fullfillment of the requirements for the

degree of

Doctor of Philosophy

By

SOMA DE
Norman, Oklahoma
2010

Time Dependent radiative Transfer Applications on Core collapse Supernova and Cosmic recombination

A Dissertation Approved for the
Homer L. Dodge Department of Physics and Astronomy

By

Dr Edward Baron (Chair)

Dr John Cowan

Dr David Branch

Dr Richard C. Henry

Dr S. Lakshmivarhan

Acknowledgments

This work was supported in part by NSF grant AST-0707704, Department of Energy Award Number DE-FG02-07ER41517, and by SFB grant 676 from the DFG. This research used resources of the National Energy Research Scientific Computing Center (NERSC), which is supported by the Office of Science of the U.S. Department of Energy under Contract No. DE-AC02-05CH11231; and the Höchstleistungs Rechenzentrum Nord (HLRN). We thank both these institutions for a generous allocation of computer time.

I sincerely thank my thesis advisor Eddie Baron for enormous support. I am thankful to my thesis committee for their feedback on my research.

Contents

List of Tables

List of Figures

Chapter 1

Introduction

1.0.1 Characteristics of different SNe

The ultimate goal of modern day astrophysics is to shed light on the geometry and nature of our universe. My dissertation is based on some of the astrophysical scenarios that can reveal information on our universe. Research in astrophysics and cosmology have accelerated extensively in the last few decades. There have been many new ground and space based telescopes that have unveiled the mysteries of the universe over the past few years. Among many channels to uncover the mysteries of our own universe, supernovae are certainly in the forefront. There is also the cosmic microwave background containing information from early universe. I will first introduce the reader about supernovae (SNe, hereafter) and then will also provide a brief introduction to cosmic microwave background radiation (hereafter CMB).

1.0.2 Characteristics of SNe and connection to cosmology

SNe are one of the most energetic events that are observed in the sky. They are easily observed in the nearby galaxies due to their high intrinsic brightness. Some of them also posses some very fundamental properties which could be exploited to calculate the cosmic distance scale. Below I will describe some properties of SNe.

SNe are commonly known as death of a massive star. The energy released in such events are around 10^{51} ergs and the peak luminosities of the brightest exceed 10^{43} egs/s ($\sim 10^9\ L_{M_\odot}$). A large galaxy produces several SNe per century and observers on Earth are detecting ~ 100 extragalactic events every year.Last supernova observed in our own Galaxy was in seventeenth century which is probably a good thing. The classification among SNe is primarily spectroscopic.

A Type Ia supernova is characterized by its Si II absorption line of rest frame wavelength at 6150 $\mathring{A}$in its observed spectrum. These particular type of SNe do to have hydrogen lines. They are known to be formed from some binary star systems in which a carbon-oxygen white dwarf is accreting matter from a companion until its mass reaches Chandrasekhar mass (1.4 $M_\odot$) or it merges with a companion white dwarf due to orbit decay by means of gravitational radiation (Parthasarathy et al., 2007). Either way, the ignition of carbon fusion deep down in the electron degenerate matter leads to a thermonuclear runaway followed by a nuclear burning front that propagates outward as a subsonic deflagaration, a supersonic detonation or some combination of the two. At this point the white dwarf s disrupted, the inner half transforms into iron-peak elements such as ^{56}Ni (which is very tightly bound with equal number of protons and neutrons) under nuclear statistical equilibrium. The outer half consists of intermediate mass elements such as calcium to oxygen that were produced by partial nuclear burning at a lower density. There is a strong debate on what kind of companion star is best suited to produce a Type Ia supernova (Branch

& Nomoto, 2007). In a popular scenario, so much mass piles up on the white dwarf that its core reaches a critical density of 2×10^9 g/cm^3. These particular type of SNe are popular due their *almost constant* absolute luminosity which can be used to calculate the cosmic distance scale Branch (1987). The almost constancy of their luminosity is related to the fact that they are formed from some a white dwarf around the Chandrasekhar mass. In other words, this relationship could be explored to get an idea of the geometry of the universe.

There are other types of SNe, known as the type II which are characterized by the presence of strong hydrogen line in their spectra. These supernovae occur at the end of the lifetime of a massive star, when its nuclear fuel is exhausted and it is no longer supported by the release of nuclear energy against gravity Poznanski et al. (2009). This typically occurs when the main sequence mass of the star exceeds a mass of $8M_\odot$.If the star's iron core is massive enough then it will collapse and become a supernova. The core upon collapse turn into a neutron star or a black hole. Few percent of of the gravitational energy released (total of $\sim 10^{51}$ ergs) is put into a shock that heats and ejects the outer layer of the star. The light curve typically has two parts, the brighter part is powered by diffusive release of the energy through the optically thick envelope, which is expanding and cooling almost adiabatically. Then there is the later and dimmer part of the light curve which is powered by trapped and thermalized γ-ray and positron decay products of ^{56}Co, the daughter nucleus of ^{56}Ni that was synthesized by nuclear reactions during the explosion. Type II

plateau SNe (SNe II-P) are the most frequent type of SN. Observationally they are defined by the presence of hydrogen in their spectra, and a plateau phase in their light curves (luminosity in certain optical pass bands over time). While SNe II-P are less luminous than SNe Ia, they are significantly more common, and their rate assuredly rises dramatically to a peak at redshifts 2-3 or beyond. The physics leading to their luminosity calibration is well understood, hence cosmic evolution is easier to study a priory (e.g., metallicity effects) (Baron et al., 2003). For more than 30 years, distance measurement methods using Type II SNe have been proposed and tested. Some rely on theoretical modeling, while others are mostly empirical, yet based on *relatively* well understood processes occurring in the thick hydrogen atmospheres that enshroud those SNe. Through recent methodological progress, combined with improved ground- and space-based facilities, SNe II-P offer the rich prospect of a great redshift baseline for cosmology and a valuable tracer of modes of star formation in host galaxies whose properties can be independently studied (Poznanski et al., 2009).

There are additional kind of SNe whose hydrogen envelope is stripped by strong stellar wind. Therefore they do not have hydrogen lines in their spectra. These originate from collapse of massive star who have already lost their outer hydrogen envelope. This particular type is classified as Type Ib.

All of the above objects are important if one is interested in determining the geometry of the universe and hence the evolution and fate of the current universe. Cosmology connects the study of astrophysical objects to study of the universe as a

whole.

1.0.3 Status of current research in SNe

The final goal of current astrophysics research is to constrain cosmological parameters which will predict the geometry of the universe and also constrain equation of state of dark energy. Geometry and energy content of the universe have tremendous implications for the nature of the universe and physical laws.

The most popular route to achieve this is to use the period-luminosity relationship of Cepheid and absolute magnitude of SNe Ia. At this point any evolution of type Ia properties (Branch et al., 2001) with redshift will threaten its use as standard candle or cosmic distance indicators. Therefore it is important to quantify the dispersion in SNe Ia properties. One approach is to model the formation mechanism accurately which unfortunately is very debatable. There is a strong debate between whether these form from SD (single degenerate) or DD (double degenerate) scenario. Some evidences show that they could be formed from SD scenario but nothing has been established with certainty. In addition since these are originated from death of a white dwarf which are faint enough to be not detected. This adds to the complication in observations to single out a companion of the progenitor with certainty.

This uncertainty leads to the complementary approaches of constraining the geometry of the universe by using type II SNe or core collapse supernovae which are formed due to collapse of a massive star. Synthetic spectroscopy and spectral fitting

could be used to determine distances. For type II this relies on determination of the correct flux or the intrinsic luminosity from the explosion models. Once the intrinsic flux is calculated, cosmic distance scale could be calculated from the observed luminosity. By measuring reddening in spectral features and accounting for the portion of the reddening to ionization, enables one to determine cosmic distance without much systematic uncertainty. The main factor inhibiting progress in the model based detailed spectroscopic methods is the required high S/N ratio. Only a handful of SNe are observed every year that are bright enough to be observed with the current large (8-10 m) telescopes (Howell et al., 2009).

1.0.4 Future status of SNe research

SNe type II could be observed in much larger number using the proposed large 20-40 m telescopes such as TMT/ELT/GMT and also the space based JWST (Barlow, 2009) . These will allow detection of larger number of SNe and also more distant SNe.According to the theoretical simulations, a few nights on the large telescopes will achieve the desired S/N for about 20 SNe in the redshift range 0.5-1.0. This will place substantial limits on the equation of state for dark energy. Other objects such as Cepheid, RR Lyrae and MIRA variables in the IR could be used to explore their period-luminosity relation since they will be less prone to dust and metallicity effects. JWST along with GSMT will serve this purpose (Hauser, 2010).

1.1 Cosmic Microwave Background (CMB)

When universe formed due to Big Bang around 14.5 billion years ago, it underwent an exponential expansion in next few seconds and slowed down its expansion to an uniform flow. There were many exotic particles formed at the time of universe's birth. Given the time after several seconds of Big Bang what happened and how it happened is very strongly debated, it is better understood how the universe behaved a few minutes after the Big Bang. At this point nuclei begin to form and this happened at a redshift of 10^8-10^9 and at a temperature of 10^9K (Hu, 2008). This is known as the epoch of nucleosynthesis. At this point there were just a huge number of photons (compared to the number of electrons, protons or light nuclei). At the high temperatures and densities of nucleosynthesis, radiation is rapidly thermalized to a perfect black body and the photon number density is a fixed function of the temperature. Apart from epochs in which energy from particle annihilation or other processes is dumped into the radiation, the baryon-photon number density ratio remains constant. Simple statistical mechanics calculations and some knowledge about current baryon density leads to a knowledge of this black body temperature. These black body photons since they were large in number, managed to escape the baryons when the universe expanded and cooled. In fact they were predicted to be observed now in the sky, in the microwave region of the electromagnetic part of the spectrum. This background black body photon flux is known as cosmic microwave background.

1.1.1 Status of Recent research on CMB

Original estimate of CMB temperature was given as T $\sim$ 12 K. This was done by (Gamow, 1948), (Alpher et al., 1948), (Dicke et al., 1965). Till date CMB is measured to be a perfect black body at T = 2.725 $\pm$ 0.0002K (Kashlinsky et al., 1999). CMB spectrum from COBE FIRAS instrument showed it to be perfect black body. Modern day estimates of the baryon-photon ratio also rely on deuterium (e.g. (Tytler et al., 2000)). CMB also has its own internal measure of this ratio from the acoustic peaks.

Recombination comes into play when we discuss about the future prospects of probing more information from CMB. Recombination is meant by the process when an electron is captured by a proton and forms a bound system and emits a photon as a result of the process. Bound system of electron and proton is the hydrogen atom. The timescale of this process of free electrons recombining into hydrogen atom is very short comparable to timescale of the expansion of the universe. If the universe is considered in complete thermal equilibrium and recombination is instantaneous, then free electron density is given from the Saha equation which also depends on the Baryon density (Hu, 2008). A little detailed calculation including non-local thermal equilibrium effects, angular momentum sub-states, feedback from energy from the prior He recombination leads to a more gradual recombination (Peebles et al., 2000),(Wong et al., 2006). The shape of the free electron density is also very sensitive to baryon density and a strong control factor in CMB polarization spectra (Hu, 2003).

1.1.2 Future prospects on CMB research

Future space missions could detect CMB polarization accurately enough to distinguish between between different detailed models predicting different ionization history and baryon density. The detailed calculation of CMB distortion whether it is due to lines from recombination or primordial inhomogeneity could generate signatures that were carried out onto current microwave background in the sky and could be investigated with Planck or future missions. CMB is a direct evidence that Big Bang happened and hence plays a very crucial role in the status of modern day cosmology.

Chapter 2

Summary of Chapters

2.1 Motivation

In the last chapter I discussed the status of modern astrophysics research in connection to cosmology. SNe and CMB are few of the tools that are used to extract information from the early universe. Being able to get correct and accurate cosmological distance is the holy grail of modern astrophysics. As I have discussed in chapter 1, SN type II have a great potential to provide cosmological distances with accuracies comparable to those obtained from Type Ia. This will involve the need of high S/N spectroscopy which could be obtainable from future large telescopes. Success of spectral fitting relies completely on accurate modeling of the core collapse explosions. The intrinsic luminosity of a type II SNe could be predicted from accurate modeling at a given redshift with some knowledge on metallicity. Once the intrinsic luminosity is known, the cosmic distance scale relies almost entirely on the following equation,

$$F = \frac{L}{4\pi d^2}$$

$$m - M = -5 + 5log_{10}d \tag{2.1}$$

In the above equation $m - M$ is the distance modulus, d is the luminosity distance in parsec. m is the apparent magnitude and M is the absolute magnitude. F is the

flux received at a distance of d, with intrinsic luminosity of L.

My dissertation work comes into play to address this particular issue of being able to model spectral features more accurately. The very famous peculiar SN 1987A which is the among the brightest SNe observed so far with a wealth of information, showed the Balmer line (transition between $n = 2$ and $n = 3$) whose line profile was not well produced in the synthetic spectra. Utrobin and Chugai (Utrobin & Chugai, 2005) predicted that including non-steady rate equations in the case of hydrogen will resolve this problem. Dessart and Hillier (Dessart & Hillier, 2008) incorporated the non-steady or in other words time dependent rate equations for hydrogen and published their synthetic spectra. This showed improvement on the Balmer line profile but the appearance of the very important Fe II lines near 5000 $\mathring{A}$and also features from Ca II, Ba II, CI lines around 8600 $\mathring{A}$were worse matches compared to their steady -state counterparts. This of course leads to an inconsistent picture leading one to wonder about if time dependence is essentially relevant. This question is only answered by explicitly calculating the recombination time for hydrogen from a synthetic spectra which matches the observed spectra reasonably well. In my dissertation I tend to investigate this issue with great detail which I think brings up other important factors in SN type II modeling. In sections below I summarize my work related to hydrogen recombination in SNe which will be described in detail in subsequent chapters.

2.2 Summary of Chapter 3

The basis of all the calculations presented in this chapter and also chapters after wards rely on one equation, known as the radiative transfer equation (RTE, hereafter). This equation relates the specific radiation intensity at a point in a given frequency band to the radiative and the collisional processes in the system. These processes depend on the abundance of each species in different energy levels. This equation originates from the Boltzmann equation which relies on the fact that total derivative of number of photons is zero in absence of any net creation or destruction of photons. Therefore any additional change in total derivative of photon number is given by the net processes creating or destructing photons. We describe this equation with more details in chapter 3. Now, for each species (any atom, ion, molecule at a given energy level) the abundance is related to the net rate of production of such species at that energy level. This relationship is more commonly known as the rate equation.

For our calculations we used a general purpose stellar atmosphere code `PHOENIX` Hauschildt & Baron (1999). This code solves the rate equations and RTE iteratively to solve for the radiation intensity and the level populations for different species.

In this chapter we address the particular problem of hydrogen recombination and its time scale in type II SN. We implement time -dependence in the rate equation in `PHOENIX`. We input a mass density profile such that $\rho \sim r^{-7}$ and luminosity to yield each SN model. We then change the intrinsic luminosity to create a good match between the observed and synthetic spectra. In each synthetic model besides a spectra,

we also generate other physical parameters such as free electron density, temperature, level populations as a function of optical depth. For a typical input density profile that of SN 1987 A, we start as early as 2 days since explosion and use time dependent rate equations and RTE to obtain the synthetic spectra. We proceed until day 20 since explosion which is around when the luminosity for SN 1987 A reached its maximum. We then match our synthetic spectra with observed spectra by tuning the absolute input luminosity (De et al., 2009).

We also used a typical density profile of SN 1999em to test our results until day 40 since explosion beginning at the epoch of maximum light. This serves the purpose of testing a typical core collapse SNe in its plateau phase.

In our calculations we find that Balmer line is well produced at all epochs and *only* needs time dependent rate equations at very early epochs since explosion. This conclusion is supported from spectra along with the explicitly calculated values of recombination times and spread of the recombination front. We also find that considering an almost full atom with many angular momentum states is important at all epochs. The recombination is more effective in a multi-level framework.

2.3 Summary of chapter 4

In this chapter we discuss our results on studying the effects of multi-level atom and presence of metals upon different fundamental probabilities such as photo-ionization probability, escape probability of resonant lines connecting the ground state and the

excited states, collision de-excitation probability. These probabilities show how important angular-momentum sub-states and metallicity in the environment could be in a given density background. We choose a steep density gradient and found that higher order angular momentum sub-states are important to consider in an environment where there are other metals present. We detect a suppression in the hydrogen ionization fraction upon inclusion of large number of angular momentum states in presence of metals. In absence of other metals we do not see significant change in the hydrogen ionization fraction upon inclusion of many angular momentum states.

We find that non-resonant process (2γ) that connects the same parity stats $2s$ and $1s$ states, affect the ionization fraction. The effect is significant in a metal-deficient environment. We also find that relative population of the ground state (compared to the first excited state) in hydrogen follows Saha equilibrium values at high optical depth. However the relative population of the ground state compared to excited state is not as high as one would expect naively from a 2-level non-LTE calculation at lower optical depths. The relative population is also expectantly sensitive to the presence of other metals. This is a useful information which establishes that even though 2-level atoms or 2-level equivalent atoms (where all higher levels are in statistical equilibrium between themselves) are a common framework to use which may not to very accurate especially for predictions for precision measurements (De et al., 2010).

2.4 Motivation and Summary of Chapter 5

While working on a typical density profile similar to a SN, I realized that hydrogen recombination scenario could also be treated using the same algorithmic framework (`PHOENIX`) in a cosmological scenario with the only prime difference of density being constant over space. Cosmological case will also have a large number of excess photons compared to the number of baryons (electrons, protons, H, He). This difference is consistently taken care of by writing the RTE correctly using the Hubble expansion velocity which contains the matter, radiation densities at a redshift when neutral hydrogen was formed. The expansion velocity is calculated using Hubble flow. We have calculated a snapshot model at a high redshift. The purpose of choosing high redshift is that at a higher redshift ($z = 1400$) much earlier than the recombination epoch, matter and radiation will be coupled. At this point one can make the safe assumption of matter and radiation temperature being equal. We incorporated the Compton scattering (adding an wavelength dependence to the cross section of Thomson scattering) (Hubeny et al., 2001). For our calculation at high redshift, we incorporate expansion velocities using Hubble flow. If the universe is static and matter and radiation are indeed in equilibrium, then the average radiation intensity will be a perfect black body. If the universe is expanding, photons will be decoupled from the matter and hence the thermal equilibrium between matter and radiation will not be present any longer. Therefore, one would expect to see lines from hydrogen recombination which will be strongest in the Lyman region of the spectra. We do recover these lines from

our calculation. The next step would be to study the effect of Helium recombination which occurs at a prior redshift ($z \sim 3000$).This is a work in progress and final goal is to use our time dependent RTE and rate equations to yield the time dependent ionization fraction *during* the recombination era (Sunyaev & Chluba, 2009).

Chapter 3

On the Hydrogen Recombination Time in Type II Supernova Atmospheres

This work has been done in collaboration with Eddie Baron (University of Oklahoma) and Peter Hauschildt (Hamburger Sternwarte, Genrmany). This has been published in Monthly notices of Royal Astronomical Society (De et al., 2009)

3.1 abstract

NLTE radiative transfer calculations of differentially expanding supernovae atmospheres are computationally intensive and are almost universally performed in time-independent snapshot mode, where both the radiative transfer problem and the rate equations are solved assuming the steady-state approximation. The validity of the steady-state approximation in the rate equations has recently been questioned for Type II supernova (SN II) atmospheres after maximum light onto the plateau. We calculate the effective recombination time of hydrogen in SN II using our general purpose model atmosphere code `PHOENIX`. While we find that the recombination time for the conditions of SNe II at early times is increased over the standard value for the case of a simple hydrogen model atom with energy levels corresponding to just the first 2 principle quantum numbers, the standard value of the recombination time is

recovered in the case of a multi-level hydrogen atom. We find that time dependence in the rate equations is important in the early epochs of a supernova's lifetime. The changes due to the time dependent rate equation (at constant input luminosity) are manifested in physical parameters such as the level populations which directly affects the spectra. The H_α profile is affected by the time dependent rate equations at early times. At late times, however, time dependence does not modify the level populations significantly and therefore the H_α profile is not modified significantly.

3.2 Introduction

Supernovae are one of the most widely researched objects in astrophysics. There has been much debate about the detailed physical nature of these objects, driven by the discovery of the dark energy using SNe Ia (Riess et al., 1998; Perlmutter et al., 1999). Supernovae add rich variety to the metal abundances in galaxies and are important to star formation theories. Supernova nucleosynthesis of heavy elements is responsible for galactic chemical evolution. Prior to the discovery of dark energy, supernova research was spurred on by the discovery of the peculiar Type II SN 1987A in the LMC (see Arnett et al., 1989, and references therein). Type II supernovae (SNe II) are classified by the presence of strong Balmer lines in their spectra in contrast with SNe I which lack strong Balmer lines. SNe II are due to core collapse of massive stars. SN 1987A was extremely well observed and much work has been done to explain all aspects of its spectra. The Balmer lines were not well reproduced at early

times (especially about 8 days after explosion). At first very large overabundances of the s-process elements Ba and Sc were suggested (Williams, 1987a,b; Höflich, 1988; Danziger et al., 1988). Further work showed that the Ba II and Sc II lines could be reproduced by assuming that the s-process abundances were enhanced by a factor of 5 compared to the LMC abundances (Mazzali et al., 1992).

The hydrogen Balmer line problem in many SNe II has not been accounted in a consistent manner. Dessart & Hillier (2008) summarizing their work using time-independent rate equations found that they were unable to reproduce the H_α line after 4 days in SN 1987A, 40 days in SN 1999em and 20 days in SN 1999br. Utrobin & Chugai (2005) points out the lack of a consistent physically motivated framework to explain the early epoch Balmer profile that matches with the observed line strength. Other authors followed different approaches to reproduce the observed line strengths with varying degrees of success (Höflich, 2003; Schmutz et al., 1990; Hillier & Miller, 1998; Dessart & Hillier, 2005). Utrobin & Chugai (2005) argued that the poor fit of the Balmer lines could be overcome by including time-dependence into the hydrogen rate equations. They argued that even in the intermediate layers, the recombination time increases due to Lyman alpha trapping or ionization from the first excited state. Consequently, the recombination time becomes comparable to the age of the supernova, making the steady-state approximation suspect. We numerically estimated the recombination time by directly calculating the recombination rate from the continuum into the bound states of hydrogen using H in NLTE with 31 bound states and

all other metals in LTE. We use the general purpose model atmosphere code PHOENIX developed by Hauschildt & Baron (1999). We specify the density structure $\rho \propto r^{-7}$ and assume the ejecta mass to be 14.7 $M_{\odot}$ as is appropriate for SN 1987A (Tsuruta & Nomoto, 1988). PHOENIX calculates the level populations, temperature and radiation field for successive epochs with a time interval of approximately two days. We generated our models and spectra using both time-dependent and time-independent rate equations. We calculated our recombination time for each epoch from the best fit spectra in each case. In § 2, we outline the theoretical framework for the recombination time and motivation for our work. In § 3, we discuss earlier work done to test the relevance of time-dependence in type II supernova atmospheres. In § 4, we describe the basic framework for our code and in § 5 we present our approach to compute the recombination time. In § 6 we state our results. In § 7, we analyze our results and address the question of the necessity of incorporating time dependence in the rate equations due to the increased recombination time.

3.3 Motivation

The recombination time is given by (Osterbrock, 1989)

$$\tau_r = \frac{1}{n_e \alpha_A} = \frac{3 \times 10^{12}\,\mathrm{s}}{n_e} \tag{3.1}$$

where n_e is the number density of electrons and α_A is the recombination coefficient. The Case A recombination coefficient is used for convenient comparison with Utrobin & Chugai (2005) who also assume Case A. Hummer & Storey (1987) suggest that the

Case B recombination coefficient is not appropriate for cases with Lyman α escape or with the electron densities as high as 10^8 g cm^{-3}. Thus, Case A is more relevant here and since Utrobin & Chugai (2005) use the same coefficient we will use it to facilitate comparison.

It has been recently argued by Utrobin & Chugai (2005) (henceforth UC05) that time dependence in the rate equations in a normal SN IIP atmosphere may be important due to a significant increase in the recombination time. It is well-known that in the early universe Lyman-alpha trapping and ionization from the second level increases the effective recombination time in hydrogen (Zeldovich et al., 1969; Peebles, 1968). The net recombination rate is then determined by transitions that do not emit Lyman-alpha (Lα) such as non-resonant processes or decays which are followed by the escape of a Lα photon without resonance scattering. For a hydrogen model atom with $n = 2$ (consisting of only levels $1s$, $2s$, $2p_{\frac{1}{2}}$ and $2p_{\frac{3}{2}}$), the ionization from the second level dominates the Lα escape probability or the 2γ transition probability from the $2s$ to the $1s$ level. This delays the effective recombination or lengthens the recombination time. In the case of an atom with many excited levels, recombination into the upper levels followed by fluorescence can significantly alter the ionization fraction due to the well known phenomena of "photon suction" (Carlsson, Rutten, & Shchukina, 1992). Furthermore, multi-level atoms increase the escape probability in the resonant transitions (for the higher level transitions), thus making recombination more effective. These two effects, due to multi-level atoms, could affect the recom-

bination process significantly, altering the physical conditions considered by UC05, so that there is once again efficient recombination and one should not necessarily expect any significant increase in recombination time over that given by Eqn 3.1. In the following sections we briefly describe relevant earlier work and explain why it is important to check the numerical value of the recombination time in the system. To be able to correctly calculate the recombination rate for a multilevel atom we use (Peebles, 1968)

$$-\frac{d}{dt}\left(\frac{n_e}{n}\right) = \sum \frac{(R_{nl} - P_{nl})}{n}. \tag{3.2}$$

R_{nl} is the recombination rate into any bound level characterized by the principle quantum number n and angular quantum number l, from the continuum and P_{nl} is the photo-ionization rate from any bound level into the continuum. This is similar to equation (23) of Peebles (1968). The difference is that instead of using simplified assumptions, we calculate the net recombination rate from the simultaneous solution of the rate equation and the radiative transfer equation. We then calculate the recombination time for a multi-level atom model by using

$$\tau_{rec} = \frac{n_e}{\sum(R_{nl} - P_{nl})} \tag{3.3}$$

Equation 3.3 is an equivalent way of estimating the recombination time. Utrobin & Chugai (2005) used

$$\tau_{rec} = \frac{n_e}{\frac{dn_e}{dt}} \tag{3.4}$$

to estimate the recombination time. In Eqs. 3.3 and 3.4, when the Lagrangian derivative of the free electron density with respect to time goes to zero (in the case of

ionization freeze out), the recombination time goes to infinity. This contradiction is only apparent, since this equation only computes the time-scale associated with the variable part of the free electron density. When the free electron density is constant in the Lagrangian frame, this equation implies that the time associated with any variation in the free electron density is infinite or in other words, it does not vary.

Since we are really considering just the recombination of hydrogen, in a solar mixture an alternative would be to define

$$t_{rec} = \frac{n_{H^+}}{R_{nl} - P_{nl}} \tag{3.5}$$

where n_{H^+} is the proton density in the system. The reason why the electron recombination time scales with hydrogen ion density is because we treat other elements except hydrogen in LTE or in other words the other elements do not have explicit time dependence in their ionic concentrations. Generally at the relevant optical depths, the ratio n_{H^+}/n_e is very close to 1.0, so there is almost no difference between Eqs. 3.3 and 3.5. We will therefore use Equation 3.3.

3.4 Earlier work

There have been different numerical models that treat the problem of recombination. This problem of recombination was addressed by Zeldovich et al. (1969) in the cosmological recombination epoch scenario. As noted above, Utrobin & Chugai (2005) have revived this for the case of SNe II. Dessart & Hillier (2008) calculated SNe IIP

spectra obtained treating the rate equations including time-dependent effects. We try to carefully review the effect of time-dependence in the results published by Dessart & Hillier (2008). The main idea is to check if the temporal nature of the rate equations is significantly supported by UC05's argument on the recombination time.

3.4.1 Utrobin and Chugai's calculation

UC05 used a two-level plus continuum approximation for the hydrogen atom to estimate the recombination probability and then estimate the recombination time. They argue that around $N_e > 10^8$ and neutral hydrogen number density $N_{HI} > 10^9$, the two-photon process dominates over other processes (collisional terms or the escape probability term) and the recombination probability is computed to be $< 2.0 \times 10^{-3}$. The characteristic temperature was 5000 K, the photo-ionization probability was assumed to be $\sim 10^3$ s^{-1}, and the dilution factor was taken as $W = 0.1$. Therefore the standard recombination time $(\alpha N_e)^{-1}$ gets modified to $\frac{1}{\alpha N_e w_{21}}$ which is factor of 500 higher than the standard recombination time. For a typical type II supernova with age $10^6 - 10^7$ s, the modified recombination time becomes of the order 10^7 s. To test their numerical estimate and predictions about the importance of incorporating time-dependence, UC05 treated the radiation field in the core-halo approximation and assumed the Sobolev approximation for line formation. Assuming that the SN atmosphere is very opaque in the Lyman continuum enabled them to fully determine the diffusive continuum in that frequency band by hydrogen recombinations and free-free

emissions.

At lower frequencies, between the Balmer and the Lyman edges, there is a large optical depth owing to interaction with numerous metal lines. Under these conditions UC05 assumed that absorption was given by the constant absorption coefficient from the solution of Chandrasekhar (1934).

In the visual band where the optical depth of the atmosphere is quite low, they adopted the free streaming approximation, which describes the average intensity of the continuum in the atmosphere as proportional to the specific intensity of photospheric radiation. The effective radius and temperature are given by their hydrodynamical model which was created after SN 1987A. UC05 incorporated gamma-ray deposition and included the time-dependent term in their rate equations for all species they considered.

They reproduced the H_α line that appears in the photospheric epoch in the first month of SN 1987A. They were unable to reproduce the additional blue peak that appears between day 20 and 29 which they argued was due to the Bochum event (Hanuschik & Dachs, 1988). Also they were able to reproduce the Ba II λ6142 line in SN 1987A between days 14 and 19 with LMC barium abundances. They argued that time-dependent hydrogen ionization provided higher electron densities in the atmosphere and thus made recombination of Ba III into Ba II more efficient.

3.4.2 Dessert and Hillier's work

Dessart & Hillier (2008) incorporated time dependent terms into the statistical and radiation equilibrium calculations of the non-LTE line blanketed radiative transfer code CMFGEN. They allowed full interaction between the radiation field and level populations to study the effect on the full spectrum. Dessart & Hillier (2008) discuss their findings on the ejecta properties and spectroscopic signatures obtained from time dependent simulations. They neglected time dependent and relativistic terms in the radiative transfer equation. However, they argued that inclusion of those terms would not affect their results because the importance of the time dependent terms arises primarily due to atomic physics and should not be sensitive to radiative transfer effects.

They compare their results with a sample of observations. They reported a strong and broad H_α line that closely matches the observed profile for SN 1999em in the hydrogen recombination epoch *without* the adaptation of non-thermal ionization/excitation due to ^{56}Ni at the photosphere just few days after the explosion. They were also able to reproduce the H_α, Na I D and Ca II IR triplet ($\sim$ 8500 Å) lines more satisfactorily.

Figure 16 of Dessart & Hillier (2008) compares the observed spectra of SN 1999em for 48.7 days since explosion and the spectra calculated from both time dependent and independent models for the rate equations. One may notice a significant mismatch between the time dependent model and observed spectra in certain regions where

the time independent models matches better. Around 4000 Å, the Fe I, Fe II lines are not reproduced well (Pastorello et al., 2004), similarly the C I and Ca II line strengths around 8600 Å are underestimated using the time dependent model and the line strengths are better reproduced by the time independent model. Dessart & Hillier (2008) find that time dependence is better for later epochs, from their work on SN 1999em and SN 1999br, about 30 days after explosion.

3.5 Description of PHOENIX

PHOENIX is a model atmosphere computer code that has been developed by Hauschildt, Baron and collaborators over the last two decades. Due to the coupling between the level populations and the radiation field, the radiation transport equation must be solved simultaneously with the rate equations. PHOENIX includes a large number of NLTE and LTE background spectral lines and solves the radiative transfer equation with a full characteristics piecewise parabolic method (Olson & Kunasz, 1987; Hauschildt, 1992) and *without* simple approximations like the Sobolev approximation (Mihalas, 1970). Hauschildt & Baron (1999) describe the numerical algorithms used in PHOENIX to solve the radiation transport equations, the non-LTE rate equations and parallelization of the code. PHOENIX uses the total bolometric luminosity in the observer's frame, the density structure, and element abundances as input parameters. The equation of radiative transfer in spherical geometry, the rate equations, and the condition of radiative equilibrium are then solved. This process is repeated

until the radiation field and the matter have converged to radiative equilibrium in the Lagrangian frame. In our model calculations we have not taken into account the ionization by non thermal electrons. Also time dependence was incorporated only in the rate equations. The inclusion of time dependence in the thermal equilibrium equation is implicit. Since the time dependent rate equations affect the opacities, the solution of the radiative transfer equation is affected as well. The explicit implementation of time dependence in the radiative transfer equation is beyond the scope of this work. Our goal was to specifically examine the effects of time dependence on the hydrogen Balmer lines and therefore only hydrogen is treated in NLTE. This both speeds up the calculations significantly and isolates the effects of time dependence on hydrogen.

3.6 Recombination Time Calculations

Our main motivation is to be able to explore the recombination time in a SN II atmosphere. In order to obtain the correct electron densities and level populations it is essential to make sure that the rate equations are correct even if the recombination time is actually longer or comparable to the age of the supernova. We incorporated the time dependent term in the rate equations and in our results we describe this as the time dependent case. We have performed calculations assuming both the steady-state, time-independent, (TI), approximation as well as the full time-dependent, (TD), rate equations. In most of our models we used a hydrogen model atom consisting of 31

levels. To save computing time and limit the time-dependent effects to the Balmer lines, we treated all other elements in LTE for this work. We started with a known density profile typical of a SN II with mass similar to the progenitor mass of SN 1987A ($\sim 14.7 M_{\odot}$) and luminosity ($1.015\times\ 10^{43}$ ergs) . We built a radial velocity grid with 128 layers. The location of the radial points was found from the assumption of homology, $r = vt$. `PHOENIX` then solves the radiative transfer equation and the rate equations simultaneously. This yields the temperature, radiation field, and other physical parameters such as pressure, optical depth, and electron density for each radial grid or layer. We choose the best model by tuning only the input luminosity and the input density profile by comparing the match between the synthetic and the observed spectra of SN 1987A.

We began with a time-independent model at Day 2 and generated snapshots for both the time dependent and independent cases up to Day 20 with intervals of 2 days. It is important for the time-dependent case to have the correct level populations at the previous time and consequently it was better to choose a smaller time interval (two days) to generate snapshots of the physical profile of the supernova. Our analysis was done on a Lagrangian velocity grid. Right after the explosion, the optical depth is very high in the innermost layers that are expanding with low velocity. At very high optical depth, radiative diffusion is an excellent approximation. Thus at high optical depths we replace the innermost ejecta with an opaque core and the luminosity is given by the expression for radiative diffusion at this boundary. Our initial grid has

has a velocity of ~ 3000 km s^{-1} and we gradually add deeper layers until at our final epoch of 20 days, the innermost layer has a velocity of around ~ 1000 km s^{-1}. To add new layers in the inner core we merged the outer low density, high velocity layers keeping the total number of layers constant. This way we preserved the grid size but also made sure that we have the physically relevant velocity range at all epochs of evolution.

In order to recover the results of UC05 in a simple hydrogen model atom case and also to understand the difference between the simple and multi-level model atom framework we repeated our calculations for a 4-level hydrogen atom model case with solar compositions. In order to have the correct physical conditions, we held the structure of the atmosphere (temperature and density) fixed from what we had obtained with the time-dependent multi-level hydrogen atom case for that epoch. We then solved for the time-dependent level populations and the associated radiation field.

3.7 Results

Our computations consist of three different systems at each epoch. They are the case when we have a 4-level ($n = 2$) hydrogen model atom in NLTE (in absence of any other metals) and time-dependent rate equations. We refer to this model as Case 1. Cases 2 and 3 are full calculations with 31-level hydrogen model atoms, solar compositions, and time-dependent and time-independent rate equations, respectively.

We measure the optical depth using the value $\tau_{\rm std}$ which is the optical depth in

the continuum at 5000 Å.

3.7.1 Ionization Fraction and Electron Density Profile

The two most important physical parameters for the recombination time are the ionization fraction, f_H, and the free electron density, n_e. In Figure 3.1 we present the electron density for the three different cases.

The upper panel shows the free electron density for Case 1 (where only hydrogen is present with $n = 2$ and rate equations are time dependent) over different epochs. Days 2–6 show a steady rise in the free electron density in the system as the optical depth becomes higher. The electron density declines at later epochs due to cooling and geometric dilution. These trends of high electron density at very early epochs and lower electron density at the later epochs are expected from the fact that the temperature is high at early times. At later epochs, the electron density at a given optical depth falls off due to the expansion and declining temperature. At epochs 4–6 d, the hydrogen in the system is almost completely ionized and the free electron density is the highest at this epoch. In the right plot of the top panel of Figure 3.1 we display the electron density for the epochs 14–20 d. At these epochs, hydrogen ionization is lower and recombination of hydrogen begins. This is evident from the corresponding temperature structure. Figure 3.2 displays the electron temperature of the system, which controls the free electron density and the level of ionization. The top left panel displays the temperatures for early epochs ($T \sim 8000 - 10000$ K

for epochs < 8 d). In the top right panel the temperature drops to around 5000 K and this is where the transition from the fully ionized to the partially ionized regime occurs. The recombination regime begins roughly at day 8. Between optical depths $\tau_{\rm std} = 0.01 - 0.1$, the temperature is around 5000 K for epochs later than about 8 d since explosion, thus recombination starts to take place, reducing the free electron density. For optical depths higher than $\tau_{\rm std} = 0.1$, the electron temperature is still high enough (even at later epochs) to maintain a high level of ionization. Using the values of the free electron density and the temperature structure it is easy to understand the ionization fraction for hydrogen in the system which is displayed in Figure 3.3. The optical depth is indicated using the value $\tau_{\rm std}$ which is the optical depth in the continuum at 5000 Å. Beginning at 6 d for Case 1, recombination starts to take place at optical depths $\tau_{\rm std} = 0.01 - 0.1$ causing a bumpy profile for the ionization fraction.

For Case 2, (time-dependent rate equations and multi-level hydrogen with 31 bound levels) results are displayed in the middle panel of our figures. We again refer to the middle panel of the Figures 3.1–3.3. The basic nature of the temperature structure, free electron density, and the ionization fraction are very similar to Case 1. The main difference in this case is that for the later epochs, the electron temperature is around 5000 K for optical depths $\tau_{\rm std} = 0.01 - 0.3$. Thus, the recombination front moves deeper into the expanding ejecta for the multilevel case with metals. This may be a cumulative effect due to the metals and the multiple bound levels. The

metals tend to suppress the ionization of hydrogen at higher optical depths, hence we would expect the ionization front for hydrogen to move deeper into the object. The multiple bound levels enhance the recombination at any optical depth. The ionization fraction for hydrogen follows the free electron density and the temperature profile by producing a bumpy profile between for $\tau_{\rm std} = 0.01 - 0.3$.

For Case 3, where the rate equations are time-independent with the 31-level hydrogen model atom, results are shown in the bottom panel of our plots. In this case the recombination front moves deeper inside compared to Cases 1 and 2. Thus, the electron temperatures of about 5000 K are reached at optical depths $\tau_{\rm std} > 1.0$ for later epochs.

To summarize our results on the ionization fraction: 1) In all three cases we observed that the results from the free electron density, electron temperature and ionization fraction are consistent with each other. 2) As the supernova expands, the recombination front moves deeper inside. The span of the recombination front is different in all three cases, being largest in Case 3. Overall, the free electron densities are similar in all three cases. 3) In the recombining regime, the electron density drops, causing a drop in the ionization fraction as well. 4) All three cases (31 level time dependent, 31 level time independent and 4 level time dependent) have visibly different ionization fraction profiles, but the difference decreases between Cases 2 and 3 (31 level hydrogen model). The ionization fraction in these models after 10 days is higher than that in the 4 level hydrogen atom time dependent model (Case 1).

5)In the recombination regime, there are glitches at the recombination front which probably arise from the imperfect spatial resolution of the ionization front. It is clear from the figures that the glitches do not affect the overall qualitative results.

3.7.2 Spectral comparison

Spectra are important as they are the only observable. In our discussion we emphasize the H_α profile of the spectra. In Figure 3.5 we present the comparison between the H_α line profile of the spectra for the Cases 2 and 3. In this plot we have days 4, 6, and 8. We used *dotted* lines for Case 3 and solid lines for Case 2 in all our line profile and spectral comparison plots. The early H_α profiles do not show any differences between Cases 2 and 3. From Day 6 onwards we notice that the line profile gets wider for Case 2 — the time dependent case. Figure 3.7 shows a spectral comparison between Cases 2 and 3. Overall, the spectral features for the Case 2 are somewhat broader (especially between $4000 - 6500$ Å).

We plot the H_α profile for days 10, 14, 16, and 20 for Cases 2 and 3 in Figure 3.6. We see a similar broadening in the profile for Case 2 except at day 16. This broadening becomes more obvious if one looks at the spectral plot (Figure 3.8). The spectra seem to have somewhat broader features for Case 2, especially in the regime $\lambda < 4500$ Å and $\lambda > 8000$ Å. We emphasize that these spectral profiles for SN 1987A were generated by independently tuning their luminosity to obtain the best fit to the observed spectra. To summarize we find that the spectral features become somewhat broader with time

dependent treatment of the rate equations, but the effect is smaller than that found by Dessart & Hillier (2008).

Figure 3.9 shows a comparison of the model spectra with observations for SN 1987A at days 4 and 6. There is a noticable improvement in the H_α profile for the time dependent case versus the time-independent case, although some of the effect is due to variations in the luminosity which is a parameter in our models. Thus, time dependent effects can be important for the early epoch H_α profiles.

3.7.3 Results

The recombination time is a crucial quantity. As noted above, the semi-analytic result is for a two-level atom and the effects of both non-resonant de-excitations and a reduction in the escape probability due to more channels could alter the numerical values compared to the simpler analysis. Figure 3.4 shows the recombination time for Cases 1 and 2.

Case 1, shown in the upper panel of Figure 3.4, the recombination time (referred as $\tau_{H(4)}$) follows an inverted profile compared to the ionization fraction (see Figure 3.3). This is consistent with the fact that the low ionization fraction will reduce recombination, resulting in a longer recombination time. Similar to the profiles for the ionization fraction and the electron density, the recombination time also gives a bumpy structure in the recombining region. For epochs > 6 d the recombination time is around $10^6 - 10^7$ for $\tau_{\rm std} = 0.01 - 0.1$. Below the recombining regime, the

recombination time is lower. This is due to the increasing density. At lower $\tau_{\rm std}$, the recombination time increases because the electron density declines.

The bottom panel of Figure 3.4 shows the recombination time for Case 2. The numerical value of the recombination time, $\tau_{H(31)}$, is highest for the earliest epochs. This is because there is barely any recombination since the temperature is $T > 10^4$ K (see Figure 3.2). In other words, the net $\frac{dn_e}{dt}$ is small causing $\tau_{H(31)}$ to increase. This high value of $\tau_{H(31)}$ is expected since the plotted regime is completely ionized for day 4 for Case 2 (see Figure 3.3). After the initial expansion, the electrons recombine. Consequently $\tau_{H(31)}$ steadily starts to rise at later epochs.

To summarize: 1) $\tau_{H(31)}$ and $\tau_{H(4)}$ following the expected profile from their respective free electron density and temperature almost follow an inverted profile compared to the ionization fraction. In other words, the recombination time is found to be proportional to the free electron density and temperature and inversely proportional to the ionization fraction.

2) The recombination time is higher for low optical depths. There is a break in the monotonic decline in the recombination time (as it moves toward higher optical depth) in the recombining regime. There is a rise in the recombination time in this regime. For optical depths $\tau_{\rm std} > 1.0$, both t_{rec} and $\tau_{H(4)}$ decrease monotonically due to the increase in the free electron density.

3) As the supernova expands, the recombination time at a given optical depth increases for most cases of $\tau_{\rm std} < 1$.

3.8 SN 1999em

SN1987A is one of the best observed astronomical objects. It is also a peculiar Type II supernova. It has two maxima in its light curve and it also has very steep rise to its maximum. On the other hand SN 1999em has steady rise to the maximum and a well-defined plateau. Thus, we also studied the effects of time-dependence in SN 1999em We began with the day 7 spectrum and marched forward in time until around day 40 (since explosion). We again considered a 31 level hydrogen atom and treated only hydrogen in NLTE. The departure coefficients (referred as b_i) are the ratio of the real level population density to the expected LTE level population density (Menzel & Cillié, 1937; Mihalas, 1978). Figures 3.12–3.14 display the departure coefficients for the levels $n = 1$ (ground state), $n = 2$, and $n = 3$. It is evident from our plots that time dependence is important at early times although the effect is very small. This effect diminishes with time. Also the effect is only relevant in the recombining regime. The explanation of this transient phenomenon is easier to understand in the Lagrangian frame. In a given mass element at very early times if the temperature is much higher than 5000K, the hydrogen is nearly completely ionized and the $\frac{d}{dt}$ term is very small. At very late times when the temperature falls much below 5000K, the hydrogen is mostly neutral and the $\frac{d}{dt}$ term is also small. Thus, the $\frac{d}{dt}$ term is important in the recombination regime. For our analysis of 1999em, we see this effect most important around 10 days. The effect steadily decreases with time. Our results agree with those of UC05.

In order to test the sensitivity of our results to the timestep we compared our results for SN 1999em for the case where we use a 4 day interval to that where we use 1 day interval in the time dependent rate equation for hydrogen. We found at early times, such as in the 14 day spectra, the change in the departure coefficients is within 3% in the line forming region, which is acceptable. This effect becomes even smaller at later times.

3.9 Discussion and Conclusions

We have studied the importance of time-dependence in the rate equations in a type II supernova atmosphere due to the increase in the recombination time. We also explored the effects of a multi-level atom and metals as compared to semi-analytic calculations with 2-level atoms without metals.

1) UC05 proposed that $\tau_{H(4)}$ is of the order of 10^7 s at $T \sim 5000$ K and $n_e = 10^8$ cm^{-3}. For epochs later than 6 days, we calculated $\tau_{H(4)}$ at similar electron density and temperature to be around 10^7 s ($\tau_{\rm std} \sim 0.02$). Thus, we recover the recombination time scale predicted by UC05 for the 4-level hydrogen case. An important difference between our results and those of UC05 is that we find the electron densities and temperatures which they used as photospheric conditions to occur at $\tau_{\rm std} \sim 0.02$ and not near $\tau_{\rm std} = 1.0$. Around $\tau_{\rm std} = 1.0$, the free electron density even for Case 1 is much higher and hence the recombination time is much smaller. This optical depth mismatch is due to the fact that we are looking at the continuum optical depth and

not the line optical depth. The ratio of the Balmer line opacity to the continuum opacity is $\sim 10^3$ in the recombining region.

We also address the question how the approximate analytical value of the simple 4-level hydrogen atom recombination time (calculated using $1/\alpha n_e$) compares with our calculated $\tau_{H(4)}$ generated from the solution of the radiative transfer equations. We refer to the approximate analytical recombination time for the 4-level hydrogen atom case as τ_{anal}. This allows us to determine the factor w_{21} (UC05). Figure 3.11 displays the ratio $\tau_{anal}/\tau_{H(4)}$, a direct measure of w_{21} described by UC05.

In Figure 3.10, we display the ratio of the recombination time for Case 2 to the recombination time from a simple hydrogen atom (Case 1) at the same epoch and at the same optical depth.

1) For earlier epochs ($t < 10$ d), $\tau_{H(31)}$ is smaller than $\tau_{H(4)}$ at almost all optical depths. For higher optical depths, the ratio increases and approaches unity. because the ionization fraction for hydrogen and $\tau_{H(31)}$ becomes independent of the number of bound levels. At this point the system is almost in LTE and the number of free electrons depends only on the temperature.

2) For the later epochs ($t > 10$ d), for $\tau_{\rm std} = 0.01 - 1.0$, $\tau_{H(31)}$ is smaller than $\tau_{H(4)}$. The ratio increases for higher optical depths. This is not important since $\tau_{H(31)}$ is small at high optical depth.

3) At low optical depths ($\tau_{\rm std} \lesssim 0.01$) $\tau_{H(31)}$ is smaller than $\tau_{H(4)}$.

4) For later epochs, (refer to the bottom panel of the Figure 3.10) at the recombi-

nation front, i.e where the $T \sim 5000$ K, the ratio $\tau_{H(31)}/\tau_{H(4)}$ rises. This comparatively higher recombination time in the multi-level case could be due to the fact that in the recombination regime, the real temperature structure for Case 1 differs significantly from that of Case 2. Specifically in most cases the temperature structure used in Case 1 is higher than the structure that would be obtained for Case 1 in radiative equilibrium. 5) We also conclude that the multi-level effects are important in all times whereas the time dependence effects are important in only early times.

The recombination time is found to be high and discontinuous from its natural trend only at the optical depths where the recombination front exists. But physically there is not anything different happening and rather it is just the sudden reduction of the electron density driving the estimated value of the recombination time higher. In the early early spectra of SN 1987A we find that H_α is better fit using the time-dependent formulation. The multi-level case recombination time is much smaller than the 4-level hydrogen atom model case in all regimes.

Therefore we conclude based on our spectra and estimates of recombination times, that time dependent rate equations in the supernova atmosphere are not essential due to any physical increase in the recombination time. The motivation for this work was to study the effect of time dependent rate equations on the Balmer profiles. We found that irrespective of the supernova subclass (1987A or 1999em) early Balmer features could be reproduced by independently tuning the luminosity using either time dependent or time independent rate equations.

Based on our work on SN 1999em, we find that the transient nature of the level population of hydrogen is not a crucial factor on the plateau, but it is important in the active recombining regime. This effect could be important for early features in the spectra but the steady state approximation should be valid in the photospheric phase. Of course, including time-dependence is not terribly costly numerically and thus it can be included when a time sequence is calculated.

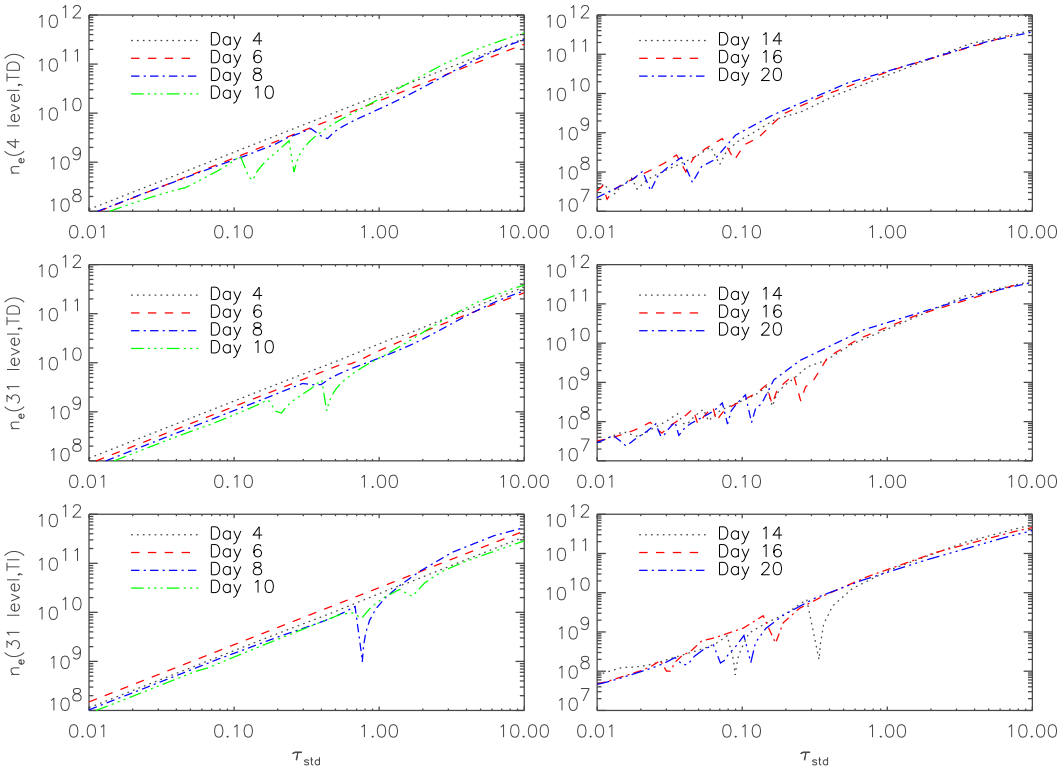

Figure 3.1 Comparison between the free electron densities at different systems. The upper panel has 4-level hydrogen atom case. The middle panel has the multilevel time dependent case. The bottom panel has the multilevel time independent case.

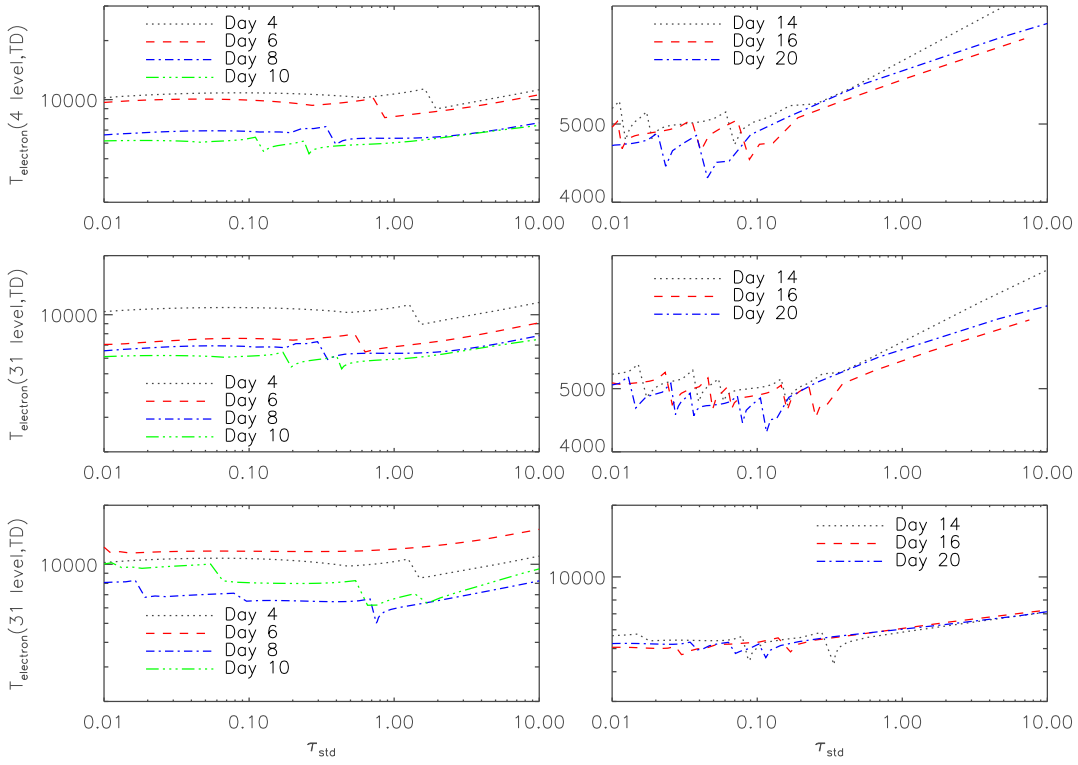

Figure 3.2 Comparison between electron temperatures at different systems. The upper panel has 4-level hydrogen atom case. The middle panel has the multilevel time dependent case. The bottom panel has the multilevel time independent case.

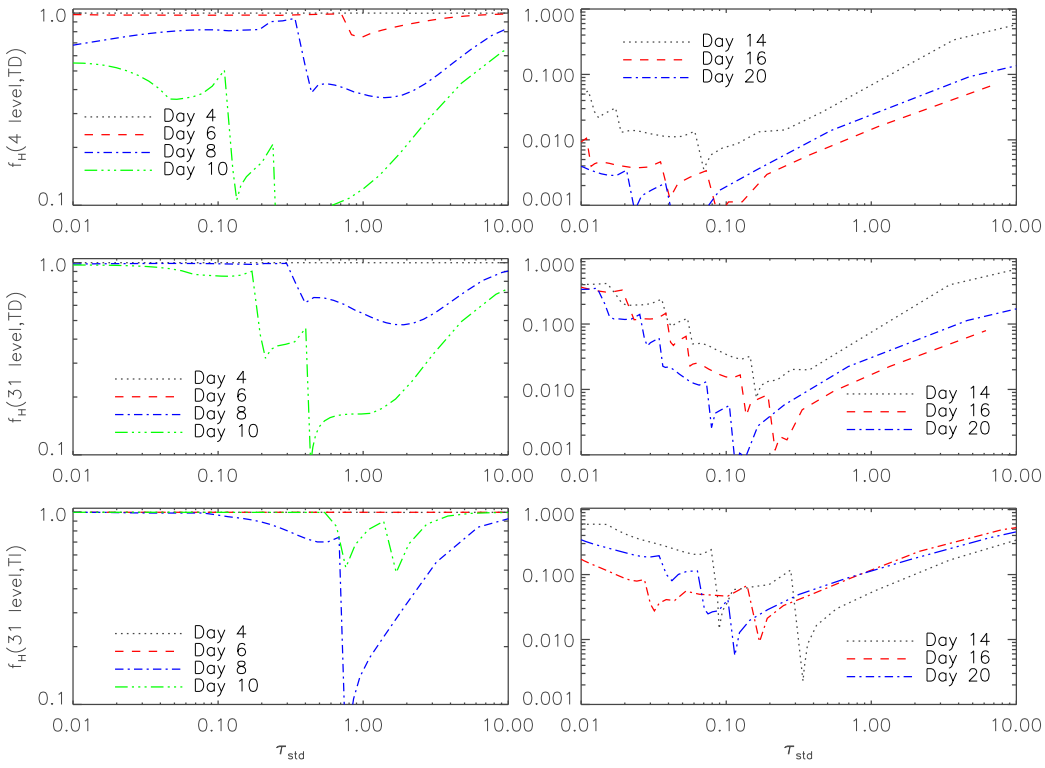

Figure 3.3 Comparison between ionization fractions at different systems. The upper panel has 4-level hydrogen atom case. The middle panel has the multilevel time dependent case. The bottom panel has the multilevel time independent case.

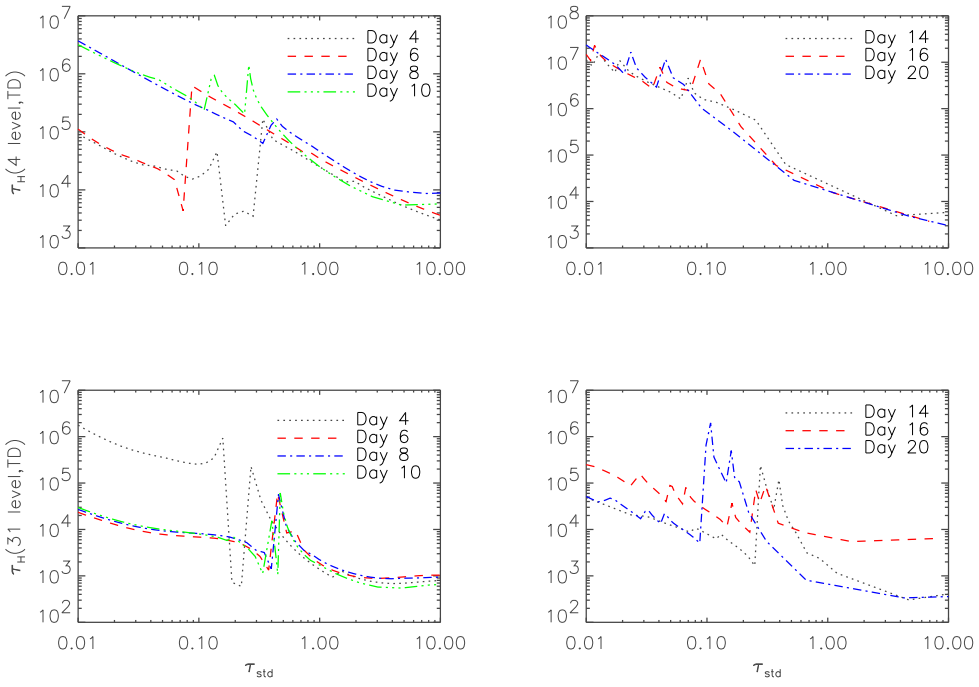

Figure 3.4 Comparison between recombination times at different systems. The upper panel has 4-level hydrogen atom case. The middle panel has the multilevel time dependent case. The bottom panel has the multilevel time independent case.

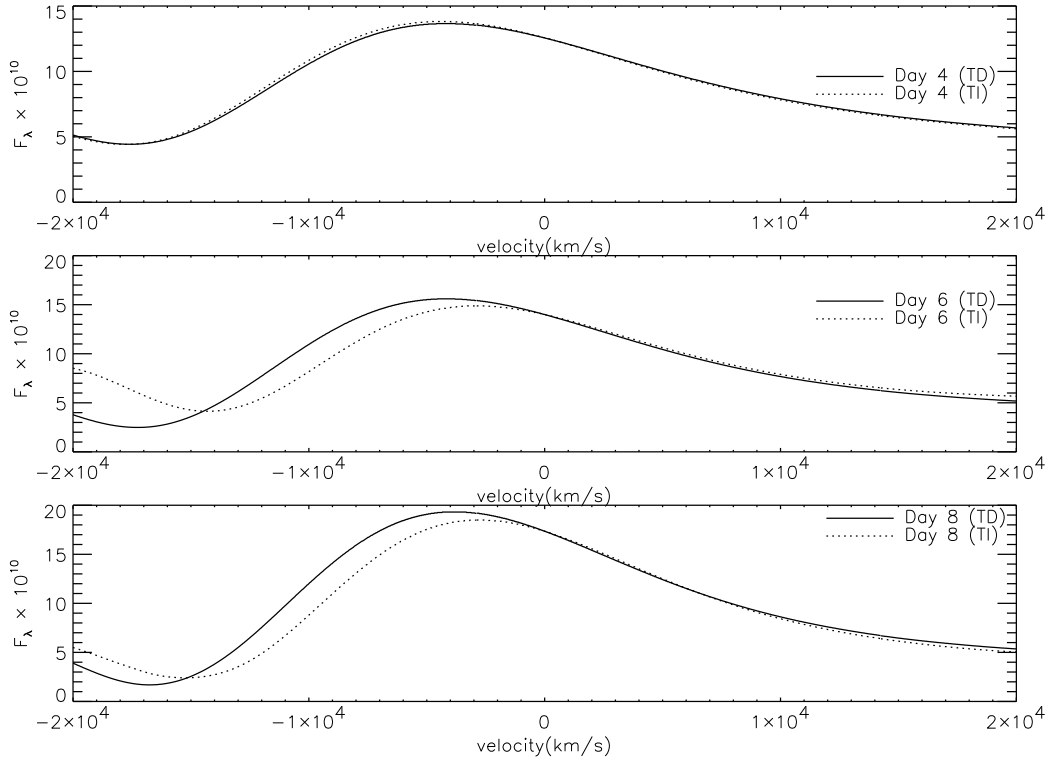

Figure 3.5 Comparison of the line profiles of H_α for Days 4, 6, 8 in the time dependent and time independent cases for a model that is appropriate to SN 1987A. The luminosity in each case has been tuned to fit the observations.

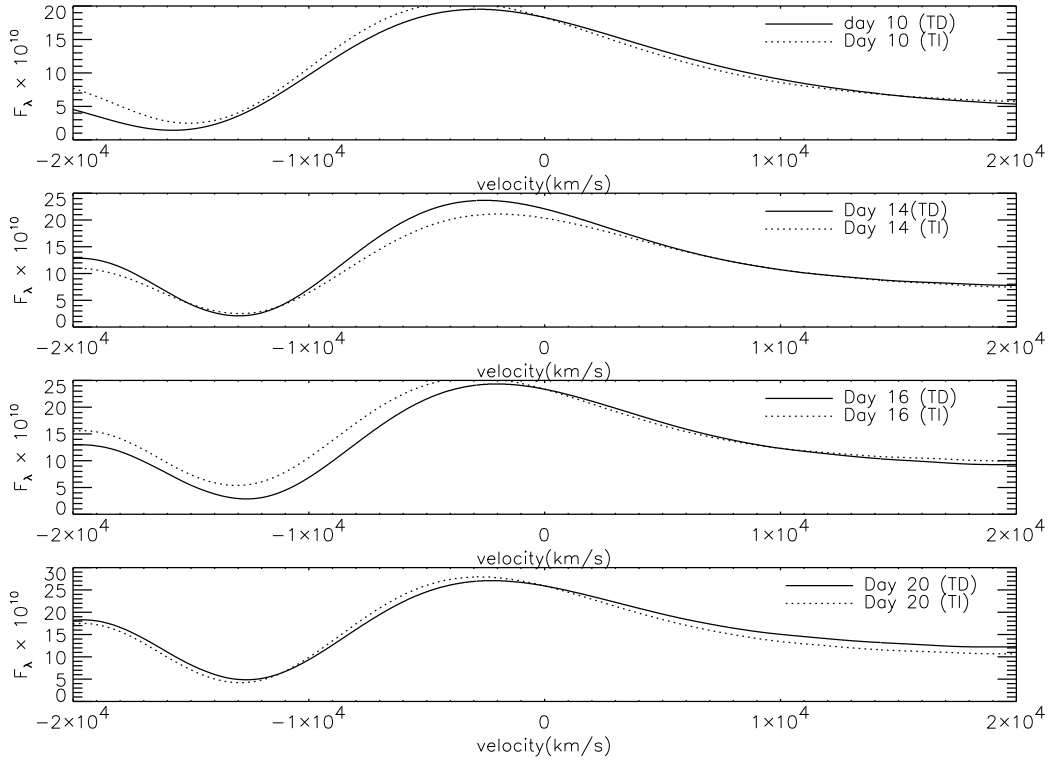

Figure 3.6 Comparison of the line profile of H_α for Days 10, 14, 16, 20 in the time dependent and time independent cases for a model that is appropriate to SN 1987A. The luminosity has been tuned to fit the observations in each case.

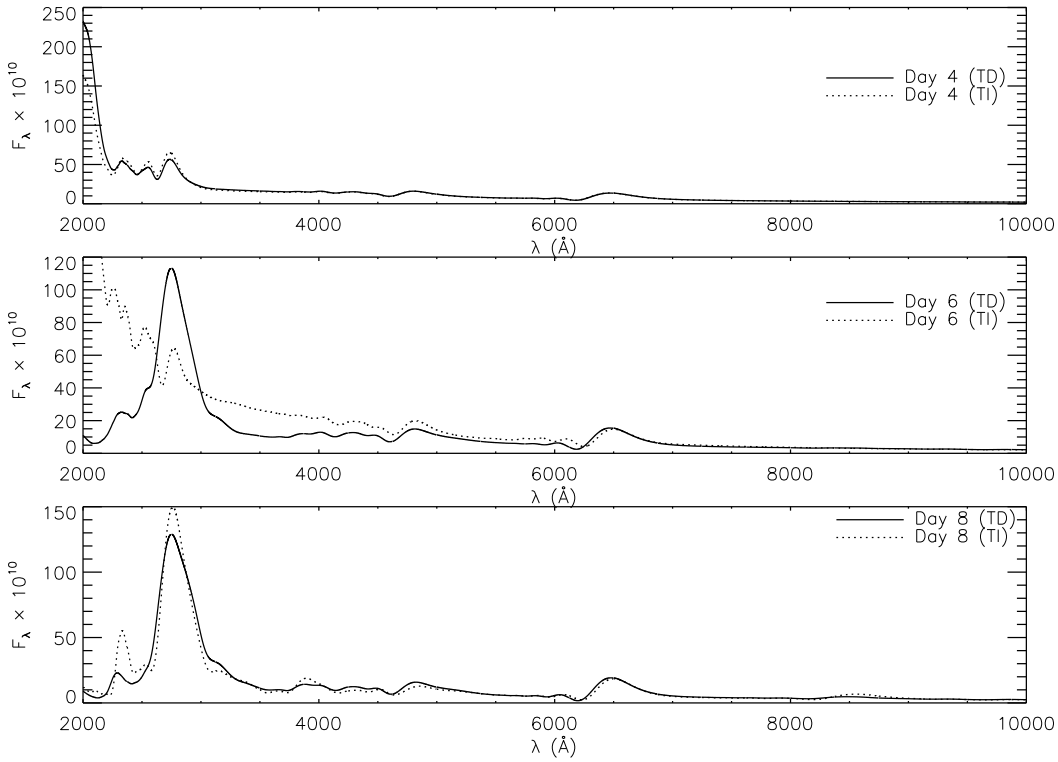

Figure 3.7 Comparison of the spectra for Days 4, 6, 8 in the time dependent and time independent cases for a model that is appropriate to SN 1987A. The luminosity in each case has been tuned to fit the observations. The differences in the day 6 UV spectra are primarily due to variations in the opacity due to the exponential dependence of the Fe II populations on the temperature and not to time dependence in the hydrogen rate equations.

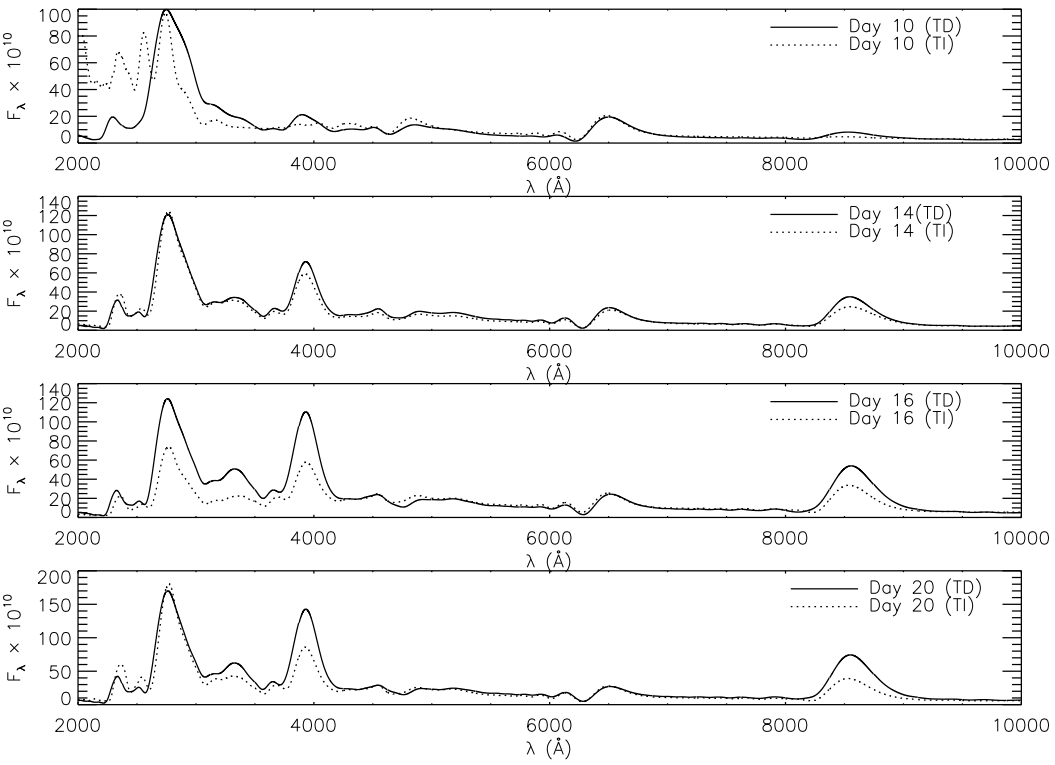

Figure 3.8 Comparison of the spectra for Days 10, 14, 16, 20 in the time dependent and time independent cases for a model that is appropriate to SN 1987A. The luminosity in each csae has been tuned to fit the observations.

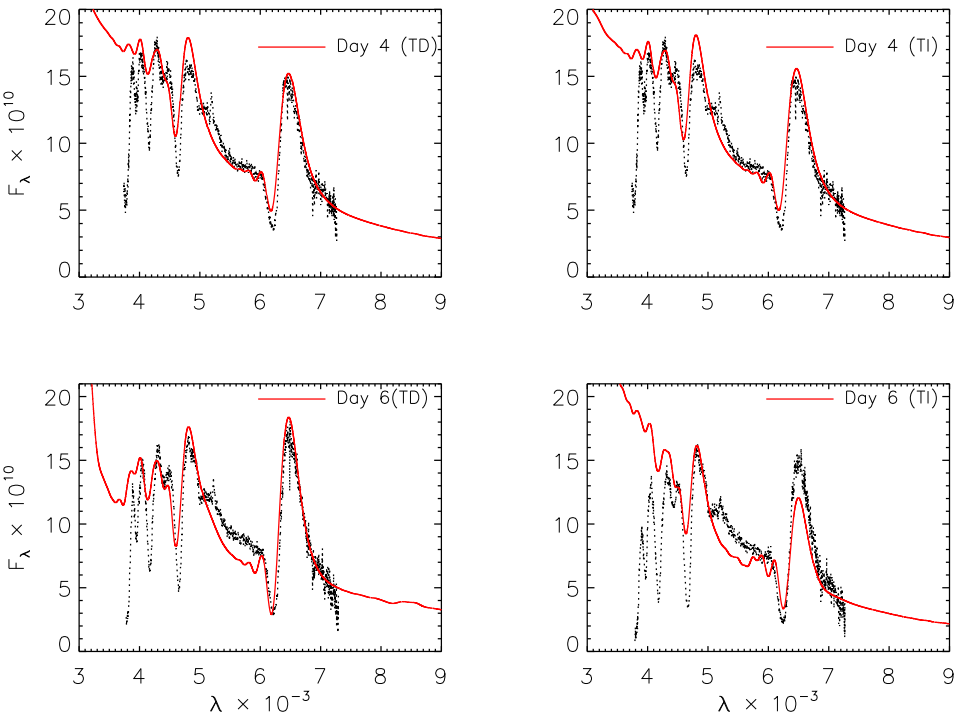

Figure 3.9 Comparison of the spectra day 4 and 6 with time dependent and time independent cases with observed spectra of SN 1987A. The luminosity in each case has been tuned to fit the observations. The H_α profile is improved in the time dependent case.

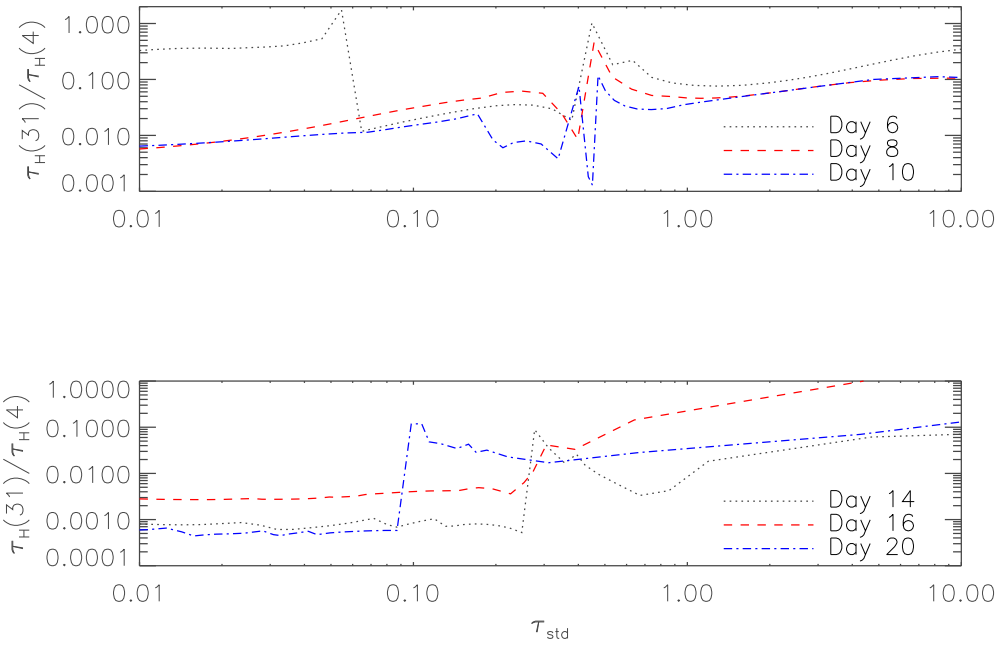

Figure 3.10 Ratio of recombination times for the time dependent multilevel hydrogen atom case and the 4-level hydrogen atom model calculated at different days. The upper panel shows the earlier epochs and the lower panel the later epochs.

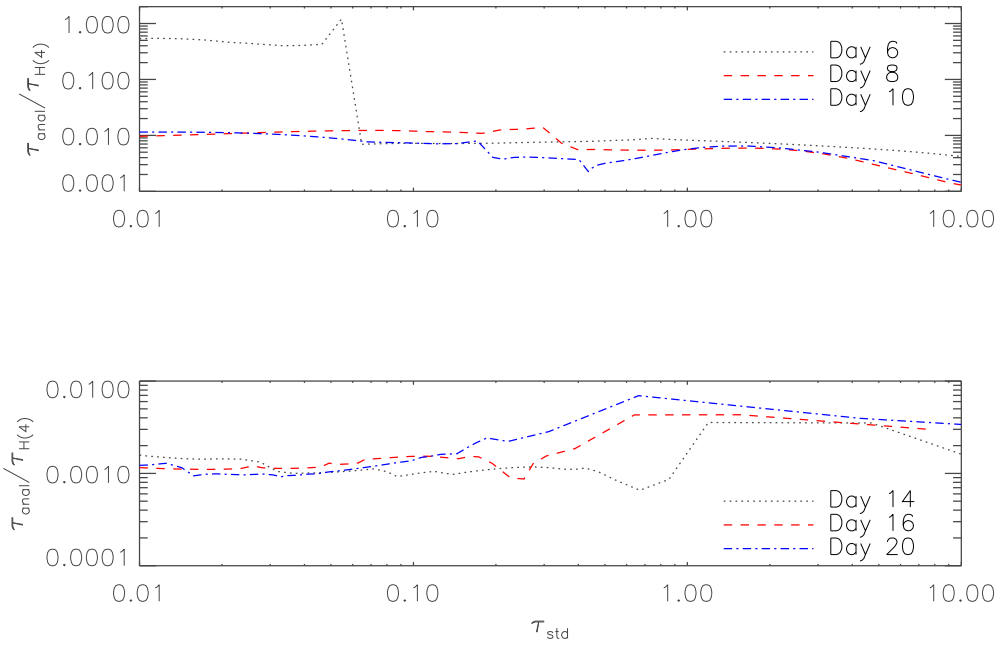

Figure 3.11 Ratio of recombination times for the analytical calculation and the 4-level hydrogen atom model calculated at different epochs. The upper panel shows the earlier epochs and the lower panel the later epochs.

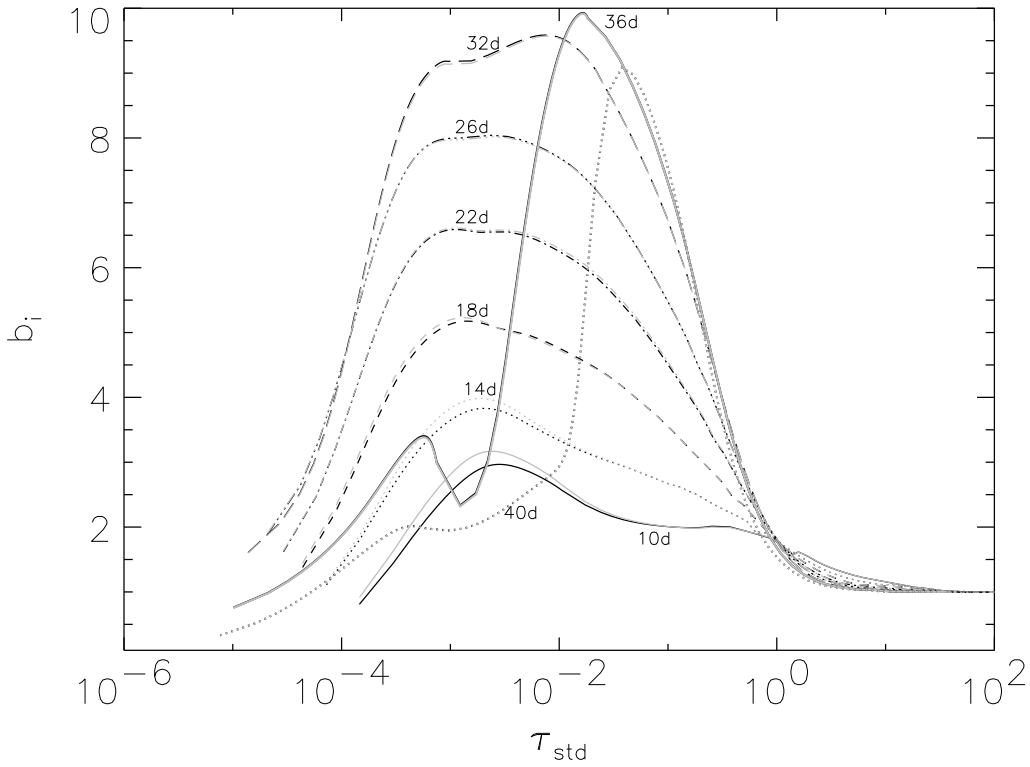

Figure 3.12 Departure coefficient, b_1, as a function of τ_{std} for the ground state of hydrogen. The black line is for the time dependent case and grey line is the time independent case for each day.

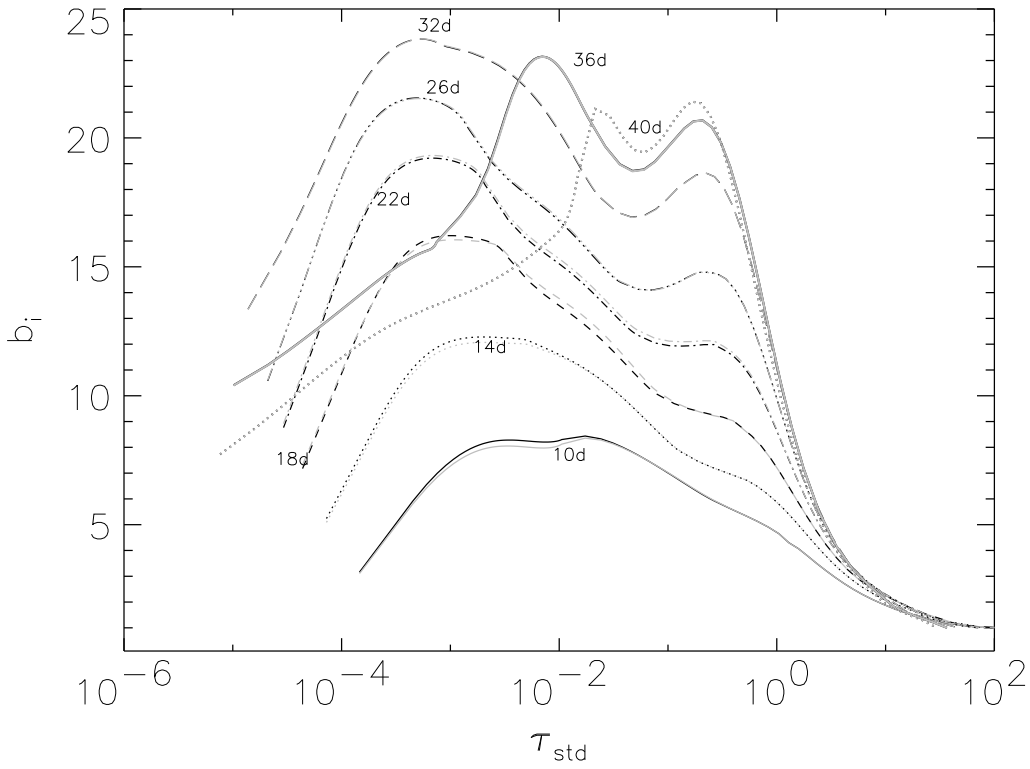

Figure 3.13 Departure coefficient, b_2, as a function of τ_{std} for the $n = 2$ state of hydrogen. The color and linestyle are same as in Figure 3.12

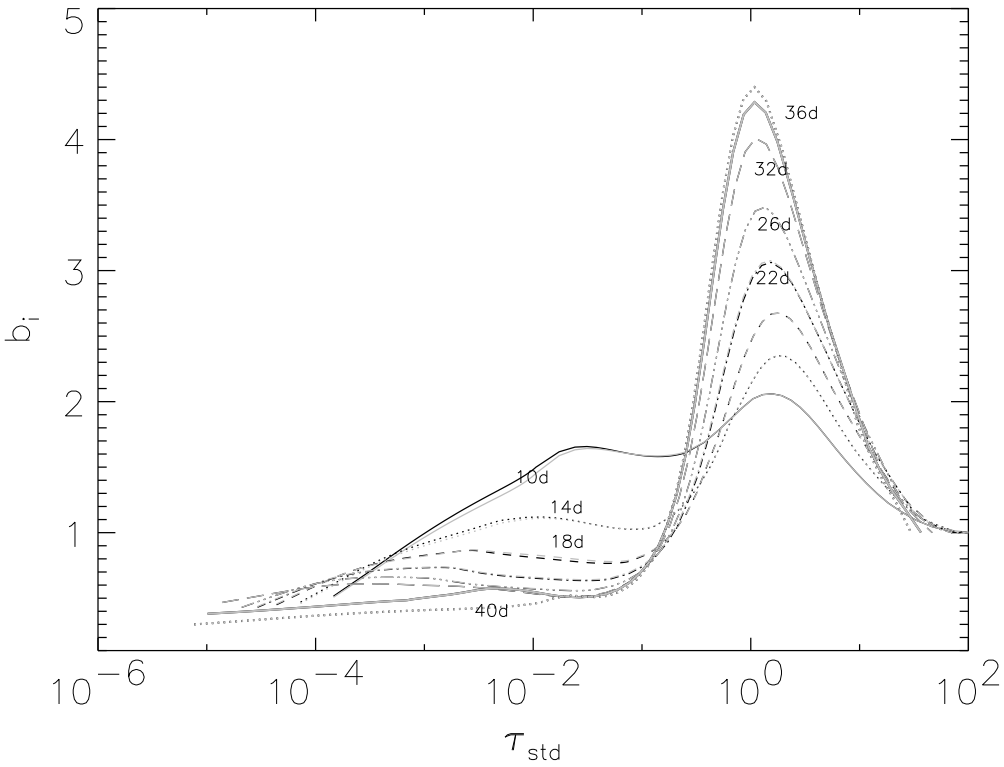

Figure 3.14 Departure coefficient, b_3, as a function of τ_{std} for the $n = 3$ state of hydrogen. The color and linestyle are same as in Figure 3.12

Chapter 4

Hydrogen Recombination with Multilevel atoms

This work has been done in collaboration with Eddie Baron (University of Oklahoma) and Peter Hauschildt (Hamburger Sternwarte, Genrmany). This has been accepted for publication in Monthly notices of Royal Astronomical Society (De et al., 2010)

4.1 abstract

Hydrogen recombination is one of the most important atomic processes in many astrophysical objects such as Type II supernova (SN II) atmospheres, the high redshift universe during the cosmological recombination era, and H II regions in the interstellar medium. Accurate predictions of the ionization fraction can be quite different from those given by a simple solution if one takes into account many angular momentum sub-states, non-resonant processes, and calculates the rates of all atomic processes from the solution of the radiative transfer equation instead of using a Planck function under the assumption of thermal equilibrium. We use the general purpose model atmosphere code `PHOENIX` 1D to compare how the fundamental probabilities such as the photo-ionization probability, the escape probability, and the collisional de-excitation probability are affected by the presence of other metals in the environment, multi-

ple angular momentum sub-states, and non-resonant processes. Our comparisons are based on a model of SN 1999em, a SNe Type II, 20 days after its explosion.

4.2 Introduction

Hydrogen recombination plays a very important role in many astrophysical phenomena such as Type II supernovae, the interstellar medium, and cosmic recombination.

Time-dependent recombination has been studied for the case of cosmological recombination (Zeldovich et al., 1969; Peebles, 1968) and for supernovae (Utrobin & Chugai, 2005; Dessart & Hillier, 2008; De, Baron, & Hauschildt, 2009). In supernovae this occurs when the hydrogen recombination time-scale becomes comparable to the age of the supernova. This effect is found to be dominant in the early epochs of the supernova's evolution (De et al., 2009). At later times, however, effects due to multi-level atom effects (the importance of having many angular momentum sub-states) become more important than time-dependent phenomena. De et al. (2009) discussed how the effective recombination timescale can be different based on time-dependent rate equations using different hydrogen atom models. The primary goal of De et al. (2009) was to determine the epoch in the lifetime of a supernova (during the photospheric phase) where time-dependence in the rate equations is most important. In doing so we found that at later times model atoms with significantly more energy levels (that is additional angular-momentum sub-states) have a strong effect in determining the effective recombination time-scale. This issue is also important for

applications other than supernovae. In fact, considering more complete atomic models is important to correctly estimate the electron density and recover subtle features in the spectra. Here, we study multi-level atomic systems for hydrogen alone using a non-LTE treatment which could alter the hydrogen ionization fraction and therefore produce a different temperature structure. We focus primarily on estimating the photo-ionization rate, the escape probability, and the collisional de-excitation rate. We show how these rates depend on the hydrogen model atom used and we also study the effects of the presence of metals on the results. These different rates ultimately lead to variations in the hydrogen ionization fraction. We also examine when the 2γ process plays the most significant role in controlling hydrogen recombination.

In § 4.3, we outline the theoretical framework relating the photo-ionization rate, collisional de-excitation rate, and escape probability to the effective hydrogen recombination time. In § 4.4, we describe our approach and different test systems that we study. In § 4.5 we present our results. In § 4.6, we state our conclusions and describe a possible framework for future work.

4.3 Theoretical Framework for Hydrogen Recombination

The ionization fraction for hydrogen is defined as

$$f_{\rm H} = \frac{n_{\rm H^+}}{n_{\rm H^+} + n_{\rm H}} \ . \tag{4.1}$$

For any system the ionization fraction depends on the net recombination rate in the system. For a system in LTE, the ionization fraction can be calculated using the Saha equation with knowledge of the electron density and temperature. On the other hand, for systems not in LTE, it is important to solve the radiative transfer equation and the rate equations simultaneously. The recombination rate of a system is dependent on the number of angular momentum sub-states of the system and also on the presence of other elements in the environment that can contribute to the free electron density. The recombination process in a system is determined by the net rate of photo-ionization and its inverse process (recombination) which are modified due to line transitions. The effectiveness (towards recombination) of a resonant transition depends on the escape probability of the line. Also there are non-radiative transitions that take place such as the collisional de-excitation of electrons to lower energy levels. In addition to these there is the downward 2γ process that connects states of the same parity while the corresponding upward transition rate is very low. Therefore it is important to study all these quantities to determine the correct nature of recombination. We investigate the 2γ process, the photo-ionization rate, the escape probability and the collisional de-excitation rates of systems with different hydrogen atom models and metallicities of the environment. We denote P_n as the photo-ionization rate from a state with index n (which is not its principal quantum number). Similarly, we define the escape probability as β_{n1} which is the escape probability for the resonant line photon between the level $1s$ and the level characterized by index n. The collisional

de-excitation rate is defined as the rate of de-excitation of the electron from level n into the $1s$ state. The analytical evaluation of each of these quantities is possible if the system is in LTE or if the system has a model atom which has just a very few angular momentum sub-states. But for a system with many angular momentum sub states (we consider 921 bound levels for hydrogen) and in the presence of metals, it is necessary to evaluate these quantities numerically from a consistent solution of the radiative transfer equation and the rate equations.

The results presented in this paper are obtained by simultaneously solving the coupled radiative transfer equation and rate equations. The rate equations use multi-level atoms including a large set of line and continuum transitions. The upward radiative rate ($i \rightarrow j$) is given as $n_i R_{ij}$ where i is a bound state and j can be a bound or continuum state. n_i is the population for level i. R_{ij} is given as (Mihalas, 1978):

$$R_{ij} = 4\pi \int_{\nu_0}^{\infty} \alpha_{ij}(\nu)(h\nu)^{-1} J_\nu d\nu \ . \tag{4.2}$$

Similarly the downward rate ($j \rightarrow i$) is calculated as $n_j(\frac{n_i}{n_j})^* R_{ji}$ where R_{ji} is:

$$R_{ji} = 4\pi \int_{\nu_0}^{\infty} \alpha_{ij}(\nu)(h\nu)^{-1} \left[(\frac{2h\nu^3}{c^2}) + J_\nu\right] e^{-\frac{h\nu}{kT}} \ d\nu \ . \tag{4.3}$$

In the above equations J_ν is the angle averaged radiation intensity at frequency ν. T is the temperature, k is Boltzmann's constant, α_{ij} is the photo-ionization cross section for the $i \rightarrow j$ transition, and ν_0 is the threshold frequency. The level populations denoted with $(*)$ are the equilibrium values as defined by Mihalas (1978). In our calculations the Sobolev approximation has not been used. In order to compare our

results with others we plot the values of the Sobolev escape probability. All the level populations were calculated without assuming the Sobolev approximation.

Below we give the equations that define P_n, β_{n1} (Mihalas, 1978). Firstly,

$$P_n = |n_n R_{n\kappa} - n_\kappa (\frac{n_n}{n_\kappa})^* R_{\kappa n}|, \tag{4.4}$$

where κ stands for the continuum level.

The escape probability β_{n1} is defined using the Sobolev escape probability as

$$\beta_{n1} = \frac{1 - e^{-\eta_{n1}}}{\eta_{n1}} , \tag{4.5}$$

$$\eta_{n1} = \frac{\pi e^2}{m_e c} f_{n1} \lambda_{n1} t \left(n_1 - \frac{g_1}{g_n} n_n \right) , \tag{4.6}$$

where f_{n1} is the oscillator strength of the line between excited level n and the ground state. n_1 and n_n are the number densities of the ground state and the excited state referred by index n, respectively. λ_{n1} is the wavelength of the line, t is the time since explosion in seconds. g_n is the degeneracy of level n and $\frac{g_1}{g_2} \sim \frac{1}{n^2}$ (Mihalas, 1978). In § 4.4 we discuss our approach to quantify the photo-ionization rate, the escape probability, and the collisional de-excitation rate.

4.4 Variation of hydrogen model atoms and composition

4.4.1 Description of the test systems

To set up the physical structure of each system we use the density profile and luminosity from a full NLTE calculation of a model atmosphere in homologous expansion, with a power-law density profile $\rho \propto v^{-7}$, 20 days after explosion, which is a reasonable fit to observed spectra of SN 1999em at that epoch. This underlying density profile and the total bolometric luminosity in the observer's frame are chosen to be representative of the conditions in SNe IIP near maximum light. Give this structure we use our general purpose model atmosphere code `PHOENIX` 1D to solve for the new temperature structure and level populations under the new conditions (such as the hydrogen model atom and the presence of other metals). The initial model of SN 1999em at 20 days after explosion was generated using a 31 level hydrogen model atom and solar metals were included. We call this starting model our base model. Our base model was generated treating hydrogen and other elements in NLTE. The details of our radiative transfer code are described in Hauschildt & Baron (1999; 2004 and references therein). The transfer equation and the rate equations were all time independent for the base model. The physical properties related to our base model are given in Table 4.1.

Now we define the different systems that we experimented upon to study the

behavior of the physical quantities affecting the recombination rate. For convenience, we name the different systems in the following way. We refer to Model A as the system which has only hydrogen and the hydrogen model atom in this case has just 4 bound states ($1s$, $2s$, $2p_{\frac{1}{2}}$,$2p_{\frac{3}{2}}$) and 4 lines that couple those states. Model C is the same as Model A, except it has a solar composition of metals present in the system in addition to hydrogen and all the other metals are treated in LTE. Model B has only hydrogen in the system but the hydrogen model atom has 921 bound levels and 995 lines that couple the bound states. Model D is the same as Model B except this has metals present and the metals are treated in LTE as in Model C. The LTE treatment of metals was chosen to reduce computing time and in a hydrogen rich environment the main role that metals play in continuum processes is to be a source of additional electrons. We did not focus on how their atomic structure affects hydrogen recombination.

For Models A and C, there are primarily three major processes considered that couple the bound states:

$$\begin{aligned} H_{1s} + \gamma &\rightarrow e^- + H^+ \ ; \\ H_{1s} + \gamma &\leftrightarrow H_{2p} \ ; \\ H_{2s} &\rightarrow H_{1s} + 2\gamma. \end{aligned}$$

In addition to this the $1s$ and $2p$ states are coupled by spontaneous transitions. In models B and D the atomic line data were taken from Kurucz (1995).

4.5 Results

We study the rates and the resulting hydrogen ionization fraction, f_H, among the four different systems that have been described in § 4.4. These different systems can have different ionization fractions primarily because the solution of the transfer equation and the resulting temperature structure will be different than in the base model. The models that have metals (Models C and D) are expected to have temperature structures similar to the base model. The 4-level hydrogen atom model without metals is likely to have a different temperature structure than the base model. These differences could be subtle but important enough to change to the hydrogen ionization fraction. In our results we have also studied whether the 2γ process has a significant effect on the recombination time scale or the resulting ionization level or the consequent temperature structure of the system.

We define τ_{std} as the optical depth corresponding to the continuum opacity at 500 nm. We classify our results depending on whether the temperature structure was held fixed at the base model value or was allowed to reach radiative equilibrium under the particular assumptions of each case, in order to isolate the effect of temperature change on the level populations and the hydrogen ionization fraction.

4.5.1 Metal-rich Models

We first discuss our results for the models where the composition included metals. We treat helium and metals in LTE. Hydrogen is always treated in NLTE. Recall that

Table 4.1 Physical characteristics from our base model.

τ	ρ (g cm^{-3})	R (cm)	v (km s^{-1})	T (K)	n_e (cm^{-3})	μ
9.897E-05	1.823E-15	2.454E+15	14200.00	3157.61	99464.3	1.34
3.626	3.084E-13	1.242E+15	7187.50	7345.20	1.079E+11	0.75
804.480	6.533E-12	4.104E+14	2375.00	26155.8	2.97E+12	0.67

The columns give various quantities as a function of optical depth. ρ is the mass density, R is the radius, v is the velocity, T is the matter temperature, n_e is the electron density, and μ is the mean molecular weight.

these systems are termed Models C and D for the 4-level and 921-level hydrogen atom models, respectively. Figure 4.1 shows the hydrogen ionization fraction for Models C and D. There is a significant change in the hydrogen ionization level, f_H, between Models C and D. The quantity f_H decreases in the multi-level atom case in the lower optical depth regime. For $\tau_{std} > 0.1$ the ionization levels among Models C and D are not very different. The quantitative difference is also tabulated in Table 4.2 which shows the physical parameters for Models C and D when the 2γ process was or was not included. The reduction in f_H due to additional angular momentum sub-states was about a factor of 3 at an optical depth of about $\tau_{std} \sim 10^{-4}$ (when the 2γ process was included in both the models). The difference in f_H decreases as the optical depth increases. In metal-rich systems, (Models C and D), the exclusion of the 2γ process

did not seem to have any significant effect for almost all optical depths of interest.

Figure 4.2 displays the net photo-ionization rate from any bound state of the hydrogen atom, P_n, for the levels $2p_{1/2}$ and $2p_{3/2}$ for Model C. The profile of P_n for Model C is not monotonic, but there is an overall trend to increase with optical depth, τ_{std}. This increase in P_n is expected due to the fact that photo-ionization dominates over recombination at higher optical depths due to higher temperatures. Figure 4.3 shows the net photo-ionization rate as a function of wave number of each energy level for Model D. Different panels show different τ_{std} regimes. The P_n values increase with increasing τ_{std} for a given energy level. Also the net photo-ionization rate does not change significantly with the change in the energy level of the bound state. There is a drop in the P_n profile at energy levels very close to the continuum. This may be due to the fact that very high energy bound states are not really distinguished from the continuum, therefore the *net* photo-ionization rate falls off.

For the calculation of the escape probability (defined as the probability for the escape of the resonant line connecting the ground state and higher energy bound state), are shown in Figures 4.4–4.5. Figure 4.4 shows the escape probability for Model C, for levels $2p_{1/2}$ and $2p_{3/2}$. The escape probability for Model C decreases with increasing optical depth and also decreases with decreasing energy of the bound state. For Model D (Figure 4.5) the escape probability increases with increasing energy of the bound state. Also the escape probability decreases very slowly with the increase in optical depth for Model D, similar to that in Model C. The apparent

difference between Models C and D is that the escape probability decreased for a higher energy level in Model C as opposed to case D where the escape probability increased with the increased energy of the bound state. For Model C, the levels in question are both $2p$ states and in Model D for those two $2p$ states we also find a slight reduction in the escape probability with increasing energy of the bound state.

The reduction in the escape probability as a function of optical depth can be explained from Eq. 4.6. At higher optical depths (for a given excited state), when n_n, the population of the excited state increases, this results in a decrease in the quantity η_{n1}. Following the decrease in η_{n1}, the escape probability β_{n1} decreases. On the other hand at a given optical depth with increasing energy of the bound state, the escape probability increases. At a given τ_{std}, for an increase in the bound state energy, n_n decreases and λ_{n1} decreases, hence the overall effect almost always is to decrease β_{n1}.

Figure 4.6 shows the collisional de-excitation rate (which is the collisional de-excitation coefficient q_e times the free electron density n_e) for Model C. In this Model there is an increase in the collisional de-excitation rate with increasing optical depth. For Model D, the collisional de-excitation rate follows a similar pattern. The increase in the free electron density with increasing τ_{std} explains the increased collisional de-excitation rate with τ_{std}. To summarize, the characteristics of the metal-rich Models C and D, 1) the ionization fraction decreases for a multi-level hydrogen atom compared to a 4-level hydrogen atom. 2) The net photo-ionization rate increases with optical depth for a given bound state. The photo-ionization rate also does not change

significantly at a given τ_{std} as the energy of the bound state increases. 3) The escape probability decreases with increasing τ_{std}, although this decrease is very small. The escape probability increases with increasing energy of the bound state except for the case of the $2p$ states. 4) The collisional rate increases with increasing optical depth. Also for the multi-level case the rate is close to the equilibrium value. 5) The 2γ process did not seem to have any significant effects in Models C and D.

4.5.2 Metal-deficient Models

In this section we focus on Models A and B. Recall that Models A and B are models where the atmosphere consists of pure hydrogen. Hydrogen was treated in NLTE in these models. In Model A, we use a 4-level hydrogen atom and in Model B, we use a hydrogen atom model with 921 energy levels. We also study how the 2γ process affects these systems when the environment is metal-free. Figure 4.7 displays the ionization fraction for Models A and B. Interestingly f_H does not change significantly between Models A and B. This is quite different when compared to Models C and D. Table 4.2 shows the changes due to the 2γ process. For Model A, at low optical depths ($\tau_{std} \sim 10^{-4}$) turning on the 2γ process produces about a 20% change in the free electron density, but for $\tau_{std} \gtrsim 10^{-3}$ no significant change is seen. For Model B, there is a significant reduction in the free electron density due to the inclusion of the 2γ process. The electron density is 5 times higher with the inclusion of the 2γ process in case B, at low optical depths, $\tau_{std} \sim 10^{-4}$. For higher optical depths, there is no

significant effect due to the 2γ process. The decrease in the free electron density due to the 2γ process is expected since the upward process is suppressed by a factor of 1/137. The change is especially noticeable in Model B. It is at a fairly low optical depth where the change in the rates observed but this is also the optical depth where the optical depth of the Balmer line is high (De et al., 2009). This wavelength regime is similar to what is described in De et al. (2009).

The net photo-ionization rate (P_n) does not change significantly between different bound states in both Models A and B (see Figures 4.8 and 4.9). Although in the multi-level case (case B), P_n increases by almost a factor of 10 from the lowest energy bound state to the higher energy bound states (except for the states very close to the continuum) at low optical depths ($\tau_{std} < 0.01$). Figures 4.10 and 4.11 show the escape probability for Models A and B respectively. The trend is very similar to that of Models C and D. The collisional de-excitation rate increases with increasing optical depths in both the Models C and D

To summarize: our findings on Models A and B (pure hydrogen models) 1) For most optical depth regimes, the basic trend in the rates is similar to Models C and D. 2)The 2γ process seems to have a significant effect in both Model A and B (at lower τ_{std}). The effect is much larger for Model B. This effect was not seen in Models C and D.

We observe the following, for almost all optical depths,

$$P_n(A) \quad > \quad P_n(C);$$

$$\beta_{n1}(A) < \beta_{n1}(C);$$

$$n_e q_{n1}(A) < n_e q_{n1}(C).$$

For Models B and D,

$$P_n(B) < P_n(D) \ (\tau < 0.01);$$

$$\beta_{n1}(B) \approx \beta_{n1}(D);$$

$$n_e q_{n1}(B) < n_e q_{n1}(D) \ (\tau < 0.01).$$

The difference in the profiles of P_n, β_{n1} and $n_e q_{n1}$ between Model A (or B) and Model C (or D) can be attributed to their different temperature profiles.

4.5.3 Metal-deficient case without temperature corrections

In our previous Models A–D, we allowed the system to reach radiative equilibrium for each assumption. It is useful to hold the temperature structure fixed and just examine the changes that are due to the variation in the compositions and model atoms. In the fixed temperature structure case we do not find a large difference as compared to the radiative equilibrium case. The differences, compared to the radiative equilibrium case occurs in the optical depth region $10^{-3} < \tau < 10^{-2}$. There is a slight suppression in the ionization fraction for Model B compared to Model A. The other rates are nearly identical.

Table 4.2 Physical characteristics from four different models, under radiative equilibrium

Model Name	Type	τ	T (K)	N_e (cm^{-3})	μ
		0.00016	2820.75	105236.	1.01
A	4 level	0.02343	4011.17	9.999E+07	1.01
		3.61	7564.24	2.351E+11	0.54
		1104.90	27565.10	3.903E+12	0.50
		0.00016	2820.61	121450.	1.01
A'	4 level, no 2γ process	0.02345	4011.18	9.999E+07	1.01
		3.61	7564.29	2.351E+11	0.54
		1106.10	26840.2	3.9035E+12	0.50
		0.00016	2801.08	3.946E+5	1.01
B	921 level	0.0272	4547.80	2.981E+8	1.01
		1.794	6779.06	1.087E+11	0.57
		1181.	20462.42	3.893E+12	0.50
		0.000157	2826.28	6.709E+4	1.01
B'	921 level, no 2γ process	0.02705	4547.69	2.983E+08	1.01
		1.794	6778.83	1.0864E+11	0.57
		1181	20462.42	3.801E+12	0.50
		0.00023	3564.79	271828.	1.26
C	4 level, metal-rich environment	4.91280	7584.85	1.260E+11	0.68
		867.030	26365.40	3.162E+12	0.625
		0.00023	3564.78	271808.	1.26
C'	4 level, metal rich environment	4.91270	7584.84	1.260E+11	0.68
	no 2γ process	867.900	26243.10	3.160E+12	0.625
		0.00011	3099.54	84640.4	1.26
D	921 level, metal rich environment	0.98338	6337.20	4.254E+10	0.98
		863.240	26109.80	3.156E+12	0.63
		0.00011	3099.46	84638.0	1.26
D'	921 level, metal rich environment	0.98373	6337.44	4.256E+10	0.98
	no 2γ process	863.080	26113.50	3.156E+12	0.63

4.6 Discussion

The primary motivation for this paper was to investigate how the multi-level structure of the hydrogen model atom affects the hydrogen ionization fraction as well as the photo-ionization, escape, and collisional de-excitation rates. We also investigated if the the metals in the environment or if the 2γ process plays a significant role in the recombination process of the system. We find that a multi-level hydrogen atom structure, or in other words a more complete set of energy levels to be important in determining the ionization profile of the system. Recently Grin & Hirata (2010) studied the effects of including a more complete set of angular momentum substates in the study of cosmological recombination and also found that including more substates to be important. The need to have a more complete set of bound states in the hydrogen atom is found to be more important in a metal-rich environment. This is because of the fact that recombination is more effective in a multi-level framework. When there is a source of additional free electrons (such as metals), the suppression in f_H is larger than in pure hydrogen models. This is merely due to the fact that the larger free electron density drives recombination, thus it is very important to use multi-level hydrogen atoms especially in realistic environments with solar compositions.

The enhancement of recombination is indicated by the increasing escape probability for the higher bound states (for both Models B and D). This is also reinforced by the almost constant photo-ionization rate over different energy bound states.

The importance of the 2γ process is seen in the 4-level pure hydrogen case (Model

A) as only a small reduction in the free electron density. In Model B, the reduction in the free electron density due to the inclusion of the 2γ process is much larger. There was not any significant effect due to the 2γ process in the solar composition Models. The larger change in Model B (at lower τ_{std}) can be explained from Figure 4.12. At low optical depths the relative population of the ground state to the first excited state is displayed. For the metal-free Models (A and B) the ratio $\frac{n_1}{n_2}$ is not very high and about 4.0 for Model B. Thus in Model B, the first excited state population is not significantly lower than the ground state population. The relative first excited state population is much lower in Models C and D (where the ratio is around $10^4 - 10^5$ at similar τ_{std}). The high level population of the first excited state (for Model B) increases the importance of the 2γ process, due to the higher number of available electrons that can recombine into the ground state and the upward transition probability for this non-resonant process being low, thus the recombination obtained is more effective. We find that it is essential to incorporate both multi-level atoms and the 2γ process. Our primary purpose was to do a simple calculation to emphasize the important factors in determining the recombination of hydrogen at typical free electron densities found in Type II supernova atmospheres. Our results show that it is important to incorporate 2γ transitions and multiple angular momentum sub-states at low optical depths where the free electron density is small (typically $\sim 10^5$ cm^{-3}) and is also typical of the free electron density during the epoch of cosmological recombination (Peebles, 1968). In H II regions the electron density is much lower making the hydrogen recombination

time scale rise. Therefore accurate treatment of hydrogen recombination is important in all of these scenarios. In the future we plan to investigate hydrogen recombination in the context of cosmological recombination epoch.

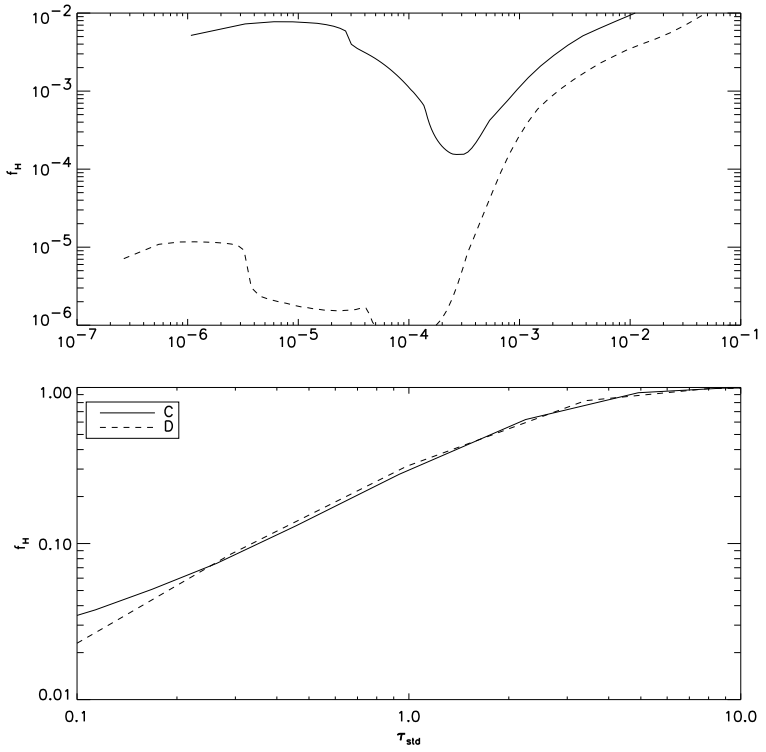

Figure 4.1 Comparison of the hydrogen ionization fraction found using the 4 level (C) and 921-level (D) model atoms in a metal-rich environment. The upper panel shows the lower optical depth regime while the lower panel shows the higher optical depth regime. We define τ_{std} as the optical depth corresponding to the continuum opacity at 500 nm.

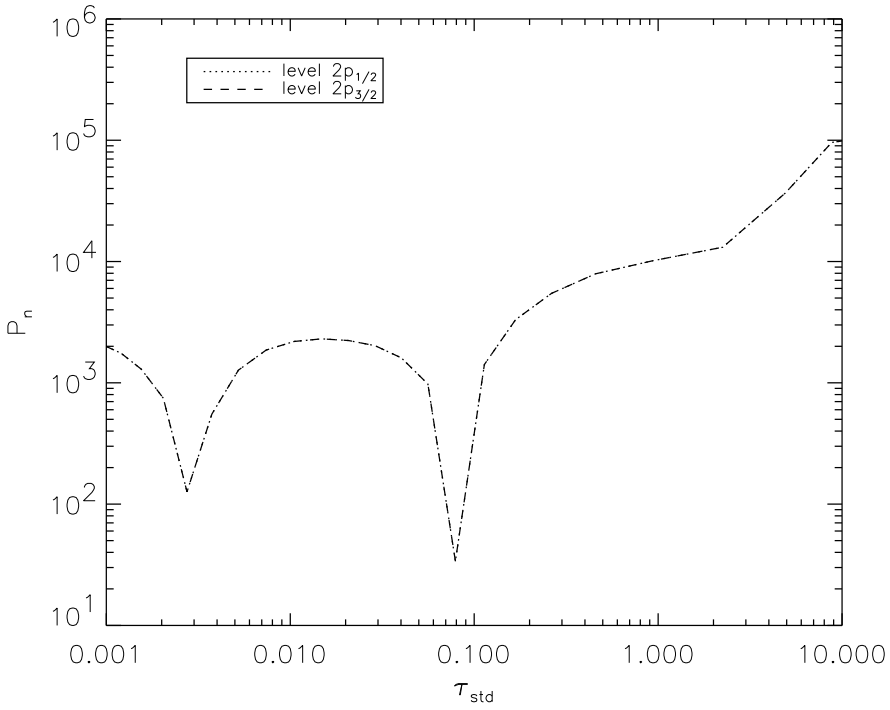

Figure 4.2 Photo-ionization rates of the $2p$ states versus optical depth for Model C.

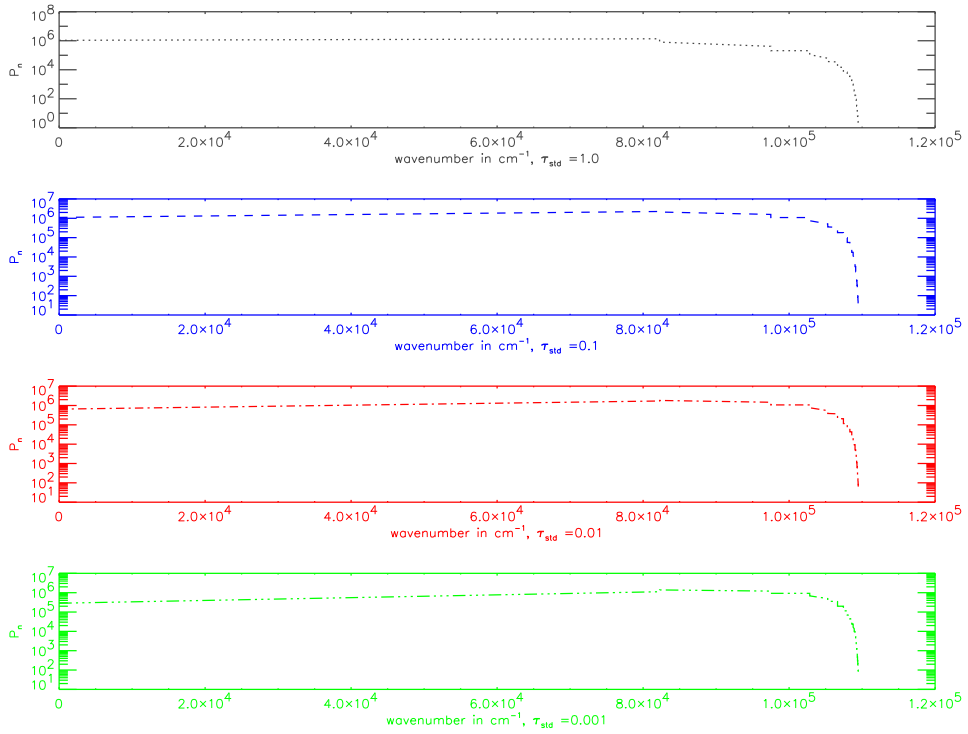

Figure 4.3 Photo-ionization rates versus energy level for Model D at different optical depths. Each panel shows a particular optical depth.

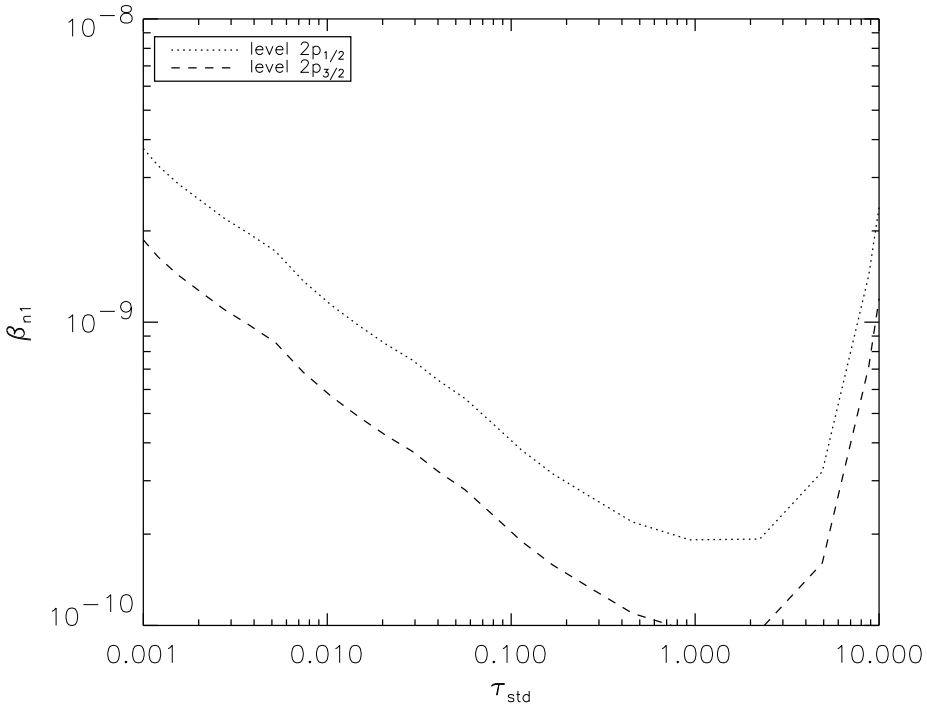

Figure 4.4 Escape probability versus optical depth for the $2p$ states for Model C.

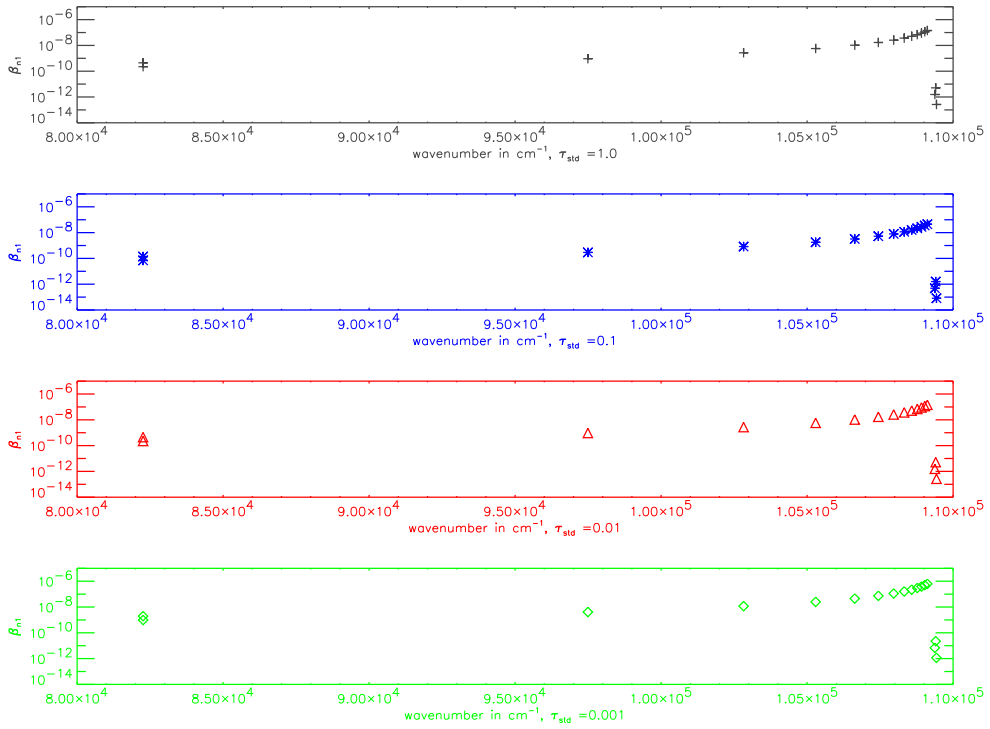

Figure 4.5 Escape probability versus energy levels for Model D at different optical depths. Each panel shows a particular optical depth.

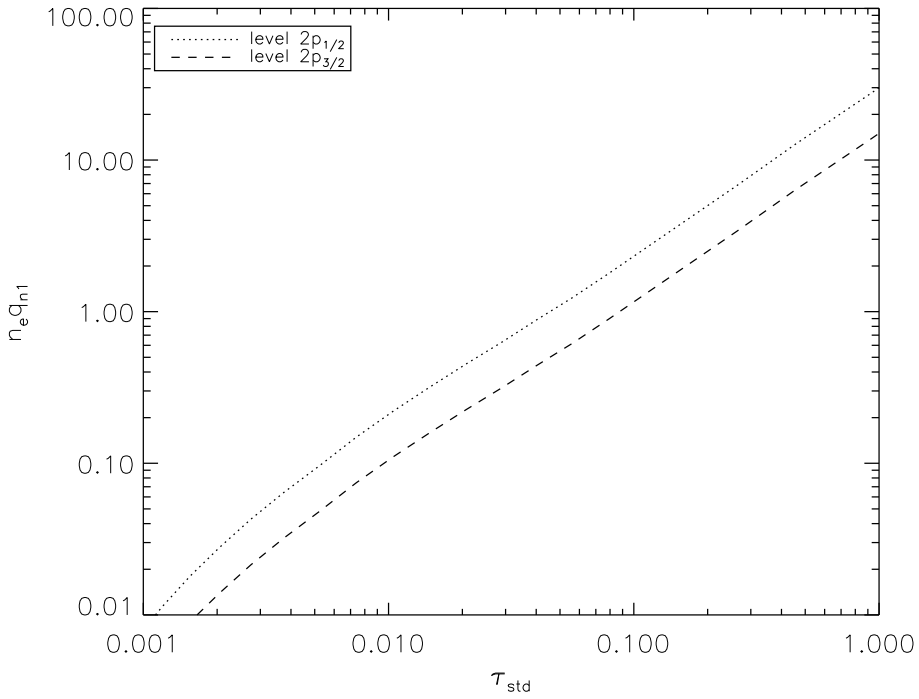

Figure 4.6 Collisional de-excitation coefficients of the $2p$ states versus optical depth for Model C.

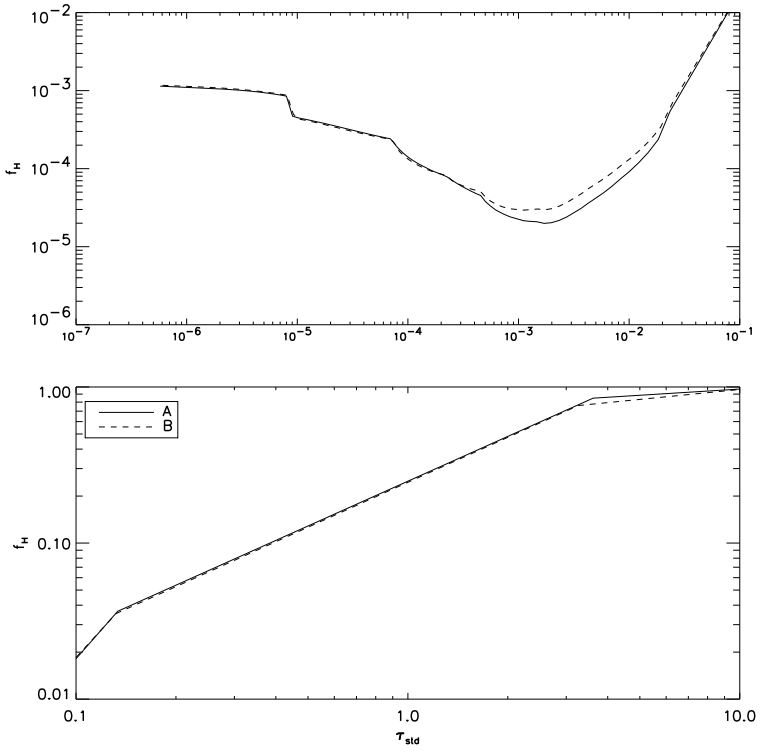

Figure 4.7 Comparison of hydrogen ionization fraction obtained using the 4 level (A) and the 921-level model (B) hydrogen atom in pure hydrogen under radiative equilibrium. The upper panel shows the lower optical depth regime while the lower panel shows the higher optical depth regime.

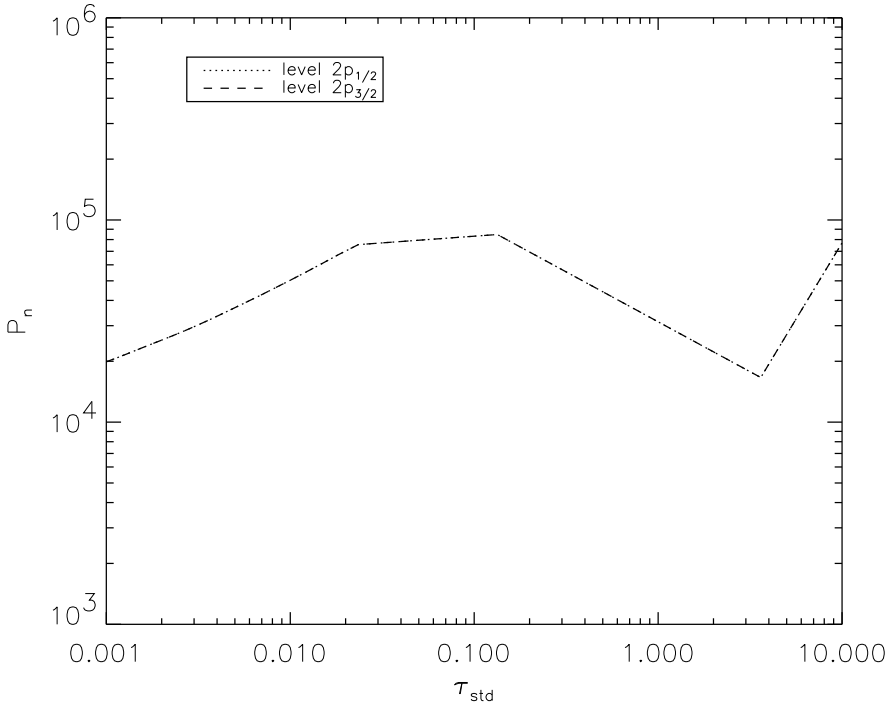

Figure 4.8 Photo-ionization rate versus optical depth for $2p$ states of Model A under radiative equilibrium. The last point at $\tau_{std} = 10$ is a numerical glitch caused by poor spatial resolution. The rate should continue to drop with depth.

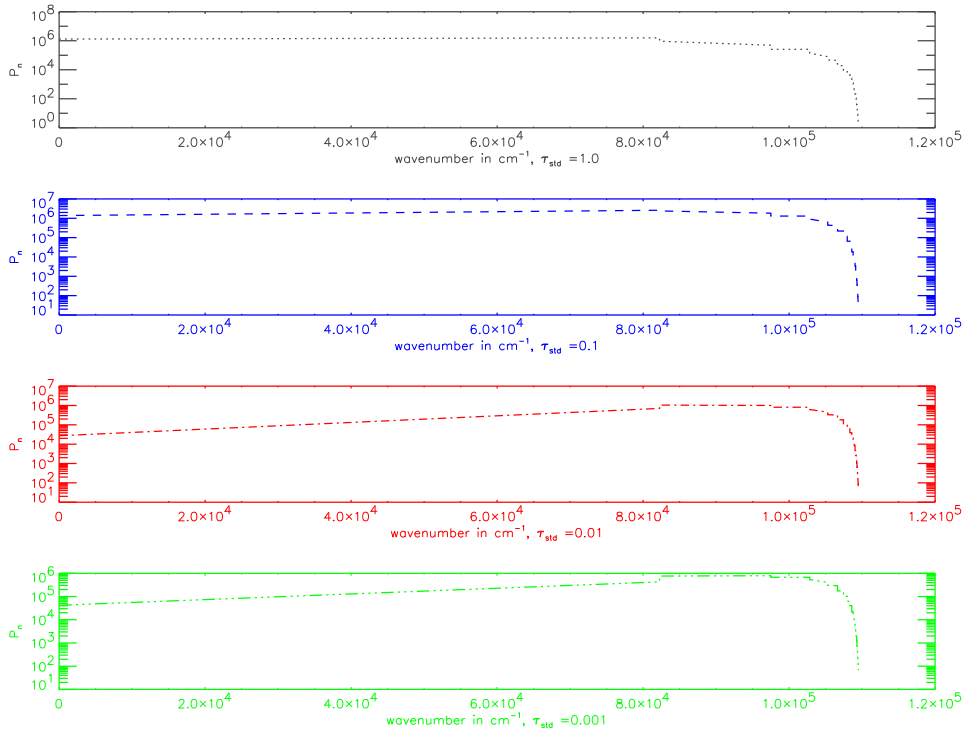

Figure 4.9 Photo-ionization rates versus energy level for Model B in radiative equilibrium. Each panel shows a particular optical depth.

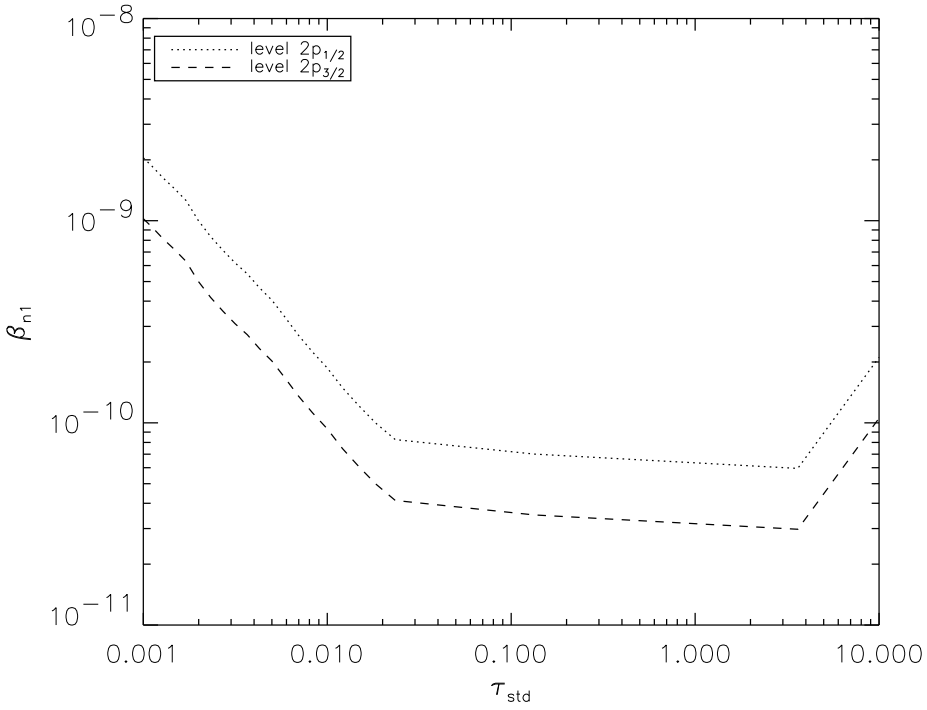

Figure 4.10 Escape probability versus optical depth for the $2p$ states of Model A in radiative equilibrium.

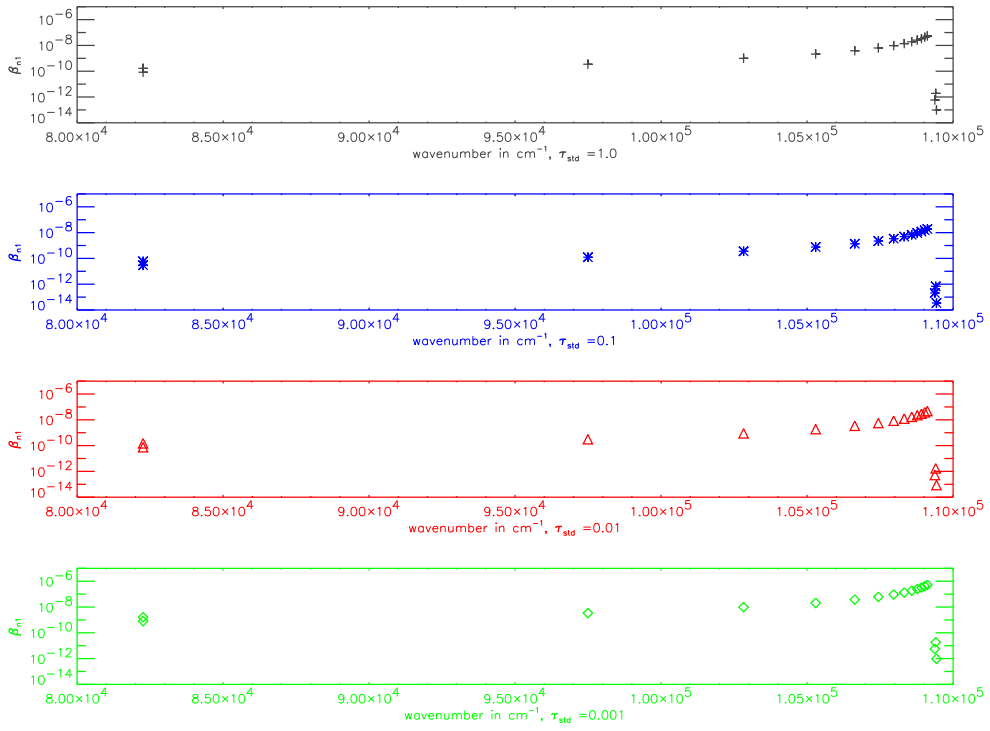

Figure 4.11 Escape probability versus energy level for Model B in radiative equilibrium. Each panel refers to a specific optical depth.

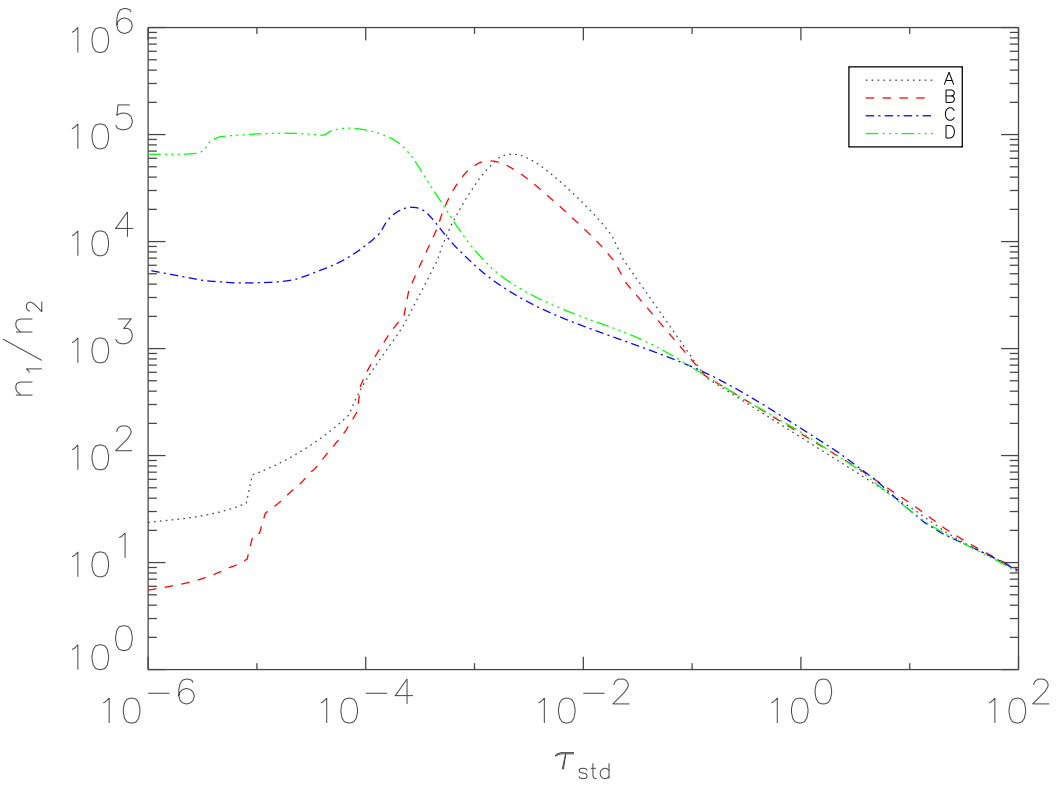

Figure 4.12 Ratio of the ground state to the first excited state population densities as a function of optical depth.

Chapter 5

Cosmic Recombination and PHOENIX

5.1 Abstract

The CMB involves primordial photons having last been scattered by neutral hydrogen about 3×10^5 years after the big bang. These photons are seen at constant temperature of about 2.7 K today. The redshifts through which the hydrogen recombination took place is between 800-1400 (Sunyaev & Chluba, 2008). Under homogeneous density conditions and in the absence of any net physical processes the distribution function of CMB follows a perfect black-body or a Planck function. Uncompensated bound-bound and bound-free interactions that release additional photons could cause unique deviation from the CMB black-body spectra ((Sunyaev & Chluba, 2009), Wong et al. (2006)). Some of the processes that are likely to affect the spectra are the escape of Lya, non resonant processes (such as 2s-1s or higher transitions), scattering by free electrons, and pre-recombination energy release due to He recombination Chluba and Sunyaev (2009). Studying these unique deviations, perhaps from the Planck mission, will provide additional direct ways to measure the primordial He abundance before stars formed, providing a better estimate of the CMB monopole temperature and specific entropy of the universe, and of the detailed ionization history of the universe, which is very important for the construction of the CMB polarization and

power spectra. In order to study the cosmic recombination epoch I have employed our radiative transfer code `PHOENIX` which is advantageous particularly because it is a time-dependent RT code. This involves starting at a redshift much higher than that of recombination redshift with a known matter density and temperature as an input. The universe is assumed to expand with only the Hubble velocity. The general relativistic RTE ((Petkova & Springel, 2009)) is then solved to evaluate the radiation temperature and intensity. For now the radiation intensity has been calculated at a redshift higher than that of recombination. In future the energy balance equation (Seager et al., 2000) will then be used to evaluate the matter temperature at the next chosen time step and process be repeated. This will yield many important quantities such as the ionization fraction as a function of time during the recombination era.

5.2 Introduction

Cosmic Microwave background (CMB) was first observed by Penzias and Wilson in 1965. The existence of CMB confirms the existence of hot Big Bang theory.CMB has been detected to be close to the perfect black body by many satellites such as the COBE FIRAS and WMAP. The observable parameters in CMB are the CMB monopole temperature, possible distortions and anisotropies on degree scales. There are some distortions that are due to the presence of primordial inhomogeneities. Also there are distortions expected due to recombination and free -free Compton scattering. In this paper we primarily address the distortion due to recombination of

hydrogen around redshift of 1100 (Scott & Smoot, 2006).

The most common way in which the CMBR spectra distortion occurs is when the photons have a blackbody spectrum in each direction but the temperature characterizing these blackbodies are different in different directions. This direction dependence of temperature is called anisotropy. The anisotropy can either be caused by a Doppler/gravitational effect or because the gas emitting the photons really did have different temperatures.

There are three processes which are important in thermalizing the CMBR in the early universe, Compton scattering, double Compton scattering and free-free scattering. Compton scattering is a rapid process but since it conserves the number of photons, it can only thermalize the energy distribution of the photons and not the number of photons. Between $z = 10^5$ and $z = 2 \times 10^6$ during which Compton scattering is efficient in thermalizing the energy distribution while other processes do not thermalize the photon number. Therefore , during this epoch energy/number ratio for photons cannot remain a blackbody. At this point since the energy to photon ratio is perturbed from that is required for the black-body, the spectrum will tend to approach a Bose Einstein distribution. The numerical values for the dimensionless chemical potential is a measure of dispersion and is expected to be much less than unity ($\sim 10^{-5}$) (Spergel, 2005).

If energy is injected into the universe after a redshift of 10^4, Compton scattering is unable to thermalize them the distribution. Since we do not observe much deviation

from the blackbody, so the energy injection must not be large. If the gas is hotter than the radiation, this distortion is produced. In the early universe when the free electron density is large, even small heating of the gas over the photon temperature (radiation temperature) may lead to large distortion of a kind, termed as Y distortion. The measure of this distortion is also less than $\sim 10^{-5}$.

Another important process in the early universe is free-free scattering which is the scattering of free electron off of a charged nucleon by either emitting by either emitting or absorbing a photon. In most cases emitting rather than absorbing. The effect of free-free scattering likely to be observed at higher wavelengths in Rayleigh-Jeans part of the CMBR. The size of these distortions are $\sim 10^{-4}$

Among all the distortions it is primarily the y-distortion which is most important and is sensitive to the baryon density. This is addressed by correct and detailed treatment of recombination. There have been significant amount of recent work done by Sunyaev and Chluba, Hirata . Most of the current work lack the proper treatment of line transfer and overlap of lines. In other words each line is treated individually. Also many of the higher angular momentum states are not resolved and are under the assumption of statistical equilibrium amongst themselves. All of these assumptions are reasonable during the thermal equilibrium at very high redshift but not during the period of recombination when additional energy is injected into the universe.. We have a radiative transfer solution framework, that has been primarily developed for stellar atmospheric calculation so far. In this paper we tend to use the solution

framework of our general purpose stellar atmosphere code PHOENIX to calculate the level populations of different species during the cosmic recombination era. We do this by iteratively solving the rate equation and the radiative transfer equation. This is a work in progress. In the next section I describe the theoretical framework for the problem and in the subsequent section I describe the preliminary results. I conclude this chapter by describing the promising aspects for future work.

5.3 Background and Basic Framework

After the Big Bang universe underwent exponential expansion known as the period of inflation. After this fast initial expansion universe slowed down its expansion. At about few minutes after Big Bang, nucleosynthesis began. At this time protons and neutrons could not anymore support each other in equilibrium and heavier nuclei started to form. Among the heavier nuclei, hydrogen, helium,deuterium and lithium are expected to form. The abundance of deuterium and Li relative to hydrogen are pretty low, being 10^{-4} and 10^{-9} respectively. This period of early light nuclei formation after Big Bang is known as the Big Bang Nucleosynthesis (BBN). This happened around redshift of $\sim 10^9$ and temperature $\sim 10^7$. Until this redshift the photons were in a very close thermal equilibrium with matter. The primordial photons are 10^9 times more in number as compared to the baryons.Therefore when these photons were thermalized and formed a perfect black body, any distortion to the black-body due to emission or absorption of photons by matter will be very small. Nevertheless

the signatures of distortion will be highly informative.

Matter and radiation were in tight thermal equilibrium though radiative Compton scattering. Due to the expansion of the universe matter and radiation started to decouple with time. As the universe cooled, the temperature dropped and free electrons recombined to form neutral helium and hydrogen. This epoch is known as the epoch of cosmic recombination. for helium,recombination happened at a much earlier redshift than hydrogen (started around $\sim$ 3000). For hydrogen the recombination took place later around redshift of 1100. The radiation and matter temperature at a redshift $z >> z_{recombination}$ will be almost equal.

$$\begin{aligned} T_r &= T_{CMB}\,(1+z) \\ T_r &= T_m \end{aligned} \tag{5.1}$$

At this redshift let's consider a piece of the universe less than the size of the observable universe by an external observer. We then grid that piece of the universe into several co moving length scales, with highest possible length scale being the size of the observable universe at that redshift. The co moving Hubble velocities are then given as (Peebles & Ratra, 2003)

$$\begin{aligned} v(r) &= H(z)r \\ \Omega_{M0}+\Omega_{R0}+\Omega_{\Lambda 0}+\Omega_{K0} &= 1 \\ H(z)^2 &= H_0^2\left(\Omega_{M0}(1+z)^3+\Omega_{\Lambda}(1+z)^{3(1+w)}+\Omega_{R0}(1+z)^4+\Omega_{K0}(1+z)^2\right) \\ 1+z &= \frac{\lambda_{obs}}{\lambda_{em}} \end{aligned} \tag{5.2}$$

The first, Ω_{M0}, is a measure of the present mean mass density in non-relativistic matter, mainly baryons and nonbaryonic dark matter. The second, $\Omega_{R0} \sim 1 \times 10^{-4}$, is a measure of the present mass in the relativistic 3 K thermal cosmic microwave background radiation that almost homogeneously fills space, and the accompanying low mass neutrinos. The third is a measure of Λ or the present value of the dark energy equivalent. The fourth, Ω_{K0} , is an effect of the curvature of space. z is the redshift.w is related to the equation of state for dark energy. For flat-space time case, $w = -1$. Also

$$\begin{aligned} \Omega_{M0} &\sim 0.28 \\ \Omega_{\Lambda} &\sim 0.72 \\ \Omega_{R0} &\sim 5.0 \times 10^{-5} \\ H_0 &= 100hkms^{-1}Mpc^{-1} \\ h &\sim 0.7 \end{aligned} \tag{5.3}$$

Due to the recombination of hydrogen, lines in the Lyman region are stronger than those in the Balmer region relative to the background continuum. Therefore one would expect to only see the Lyman features in the CMB today, and the features will be detectable in the *cm* wavelength region or the microwave part of the electromagnetic spectra. // To carefully solve the issue of cosmic recombination one must solve the radiative transfer equation and the rate equation 'together'. The radiation intensity depends on the rates of the fundamental processes and the level population of different species and vice verse. This inter-dependence makes the RTE and rate equations

highly coupled and one may approach to solve them using iterative methods. Below we state the form of RTE we use for the recombination era (Petkova & Springel, 2009),

$$a_t \frac{\partial I}{dt} + a_r \frac{\partial I}{\partial r} + a_\mu \frac{\partial I}{\partial \mu} + a_\lambda \frac{\partial \lambda I}{\partial \lambda} + 4a_\lambda I = \eta_\lambda - \chi_\lambda I \tag{5.4}$$

In the above equation $I \equiv I_\lambda$. The coefficients are described in (Castor, 1970). η_λ is the emissivity and χ_λ is the extinction coefficient in the comoving coordinates. a_λ is related to the Hubble expansion velocities. The rate equation for the population of certain species is described as

$$\frac{dn}{dt} = Source - Sink \tag{5.5}$$

In our work 5.4 and 5.5 are solved iteratively using full characteristics rays with approximate Lambda iteration method using our general purpose stellar atmosphere code `PHOENIX`. In the next section we describe how we set up the velocity and temperature structure.

5.3.1 Compton scattering

In the early universe one important process that modified the black body was Compton scattering. This is a scattering process of photons off of electrons when the frequency of the scattered photon changes as a result of the scattering. This process is described as

$$e^- + \gamma(\nu) = e^- + \gamma(\nu^{'}) \tag{5.6}$$

Compton scattering conserves the number of photons but it does not conserve the frequency distribution of photons. Therefore this process distorts the black body. It is important to include Compton scattering as it is an important process in the early universe.Below I describe how we incorporate the Compton scattering in our calculation. The framework is to include an angle averaged frequency dependent source function in the radiative transfer equation. We use the form of the source function described in (Hubeny et al., 2001). The cross section for the Compton scattering is given as

$$\begin{aligned} \sigma_\nu &= n_e \sigma_T \, (1 - 2x) \\ x &= \frac{h\nu}{m_e c^2} \end{aligned} \tag{5.7}$$

In the above equation, n_e is the free electron density, σ_T is the cross section for Thompson scattering. A simple treatment to include the effect of Compton scattering would be to replace the source function in RTE as (Hubeny et al., 2001)

$$\begin{aligned} S_\nu^{Compton} &= (1-x)J_\nu + (x - 3\Theta)J_\nu^{'} + \Theta J_\nu^{''} \\ &+ \frac{c^2}{2h\nu^3} J_\nu 2x(J_\nu^{'} - J_\nu) \\ \Theta &= \frac{kT}{m_e c^2} \\ J_\nu^{'} &= \frac{\partial J_\nu}{\partial (ln\nu)} \\ J_\nu^{''} &= \frac{\partial^2 J_\nu}{\partial (ln\nu)^2} \end{aligned} \tag{5.8}$$

In the above equations, $S_\nu^{Compton}$ is the additional source term due to the Compton scattering.J_ν is the angle averaged radiation intensity.

5.4 Steps to calculate radiation intensity

At this stage we only focus to calculate the radiation field intensity at a given redshift that is much earlier than the redshift of recombination , so one can assume the equality of matter and radiation temperature. From equation 5.1 we calculate T_m and T_r. We input matter density, Hubble velocity, matter temperature, abundances of species to solve the RTE and rate equations iteratively. This yields the values of free electron density and average radiation intensity in the comoving frame. Our framework has the 2-photon transition in hydrogen connecting the 2s and 1s levels, 31 level hydrogen atom (inclusive of angular-momentum states) and each level is resolved (ie statistical equilibrium between amongst angular momentum sub-states of higher is not assumed). In Figure 5.1 we present rest-frame radiation intensity as a function of wavelength. In the bottom panel we have the perfect blackbody and in the upper panel we have zoomed into the Lyman region where we are able to see some line features. The features are quite small compared to the background continuum.

5.5 Discussion

In our paper the main idea was to use the framework for solving the RTE and rate equations iteratively that already exists for SNe and apply it in the cosmological case,by replacing the expansion velocities by Hubble velocities. Most cosmological radiative transfer codes do not consider interference between lines, resolving higher

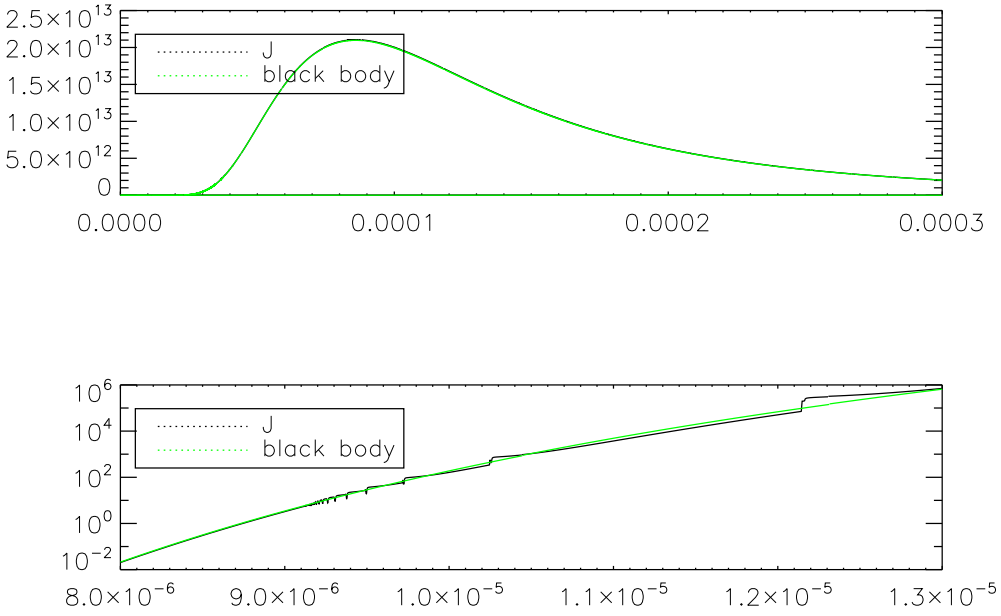

Figure 5.1 Comparison of Black body and average radiation intensity at z=1300.

angular momentum states. Our code explicitly solves the RTE and the rate equation. We also consider multi-level hydrogen and helium atoms. Future work, will be to yield time dependent free electron densities which will be useful for calculation of CMB polarization spectra. We will also look at the line features in greater detail.This calculations although very precise will be important to interpret Planck satellite data which will measure Sunyaev-Zeldovich effect which is like a direction dependent y-distortion.

Chapter 6

Conclusion

Accurate determination of ionization level in a system is a very important in precision cosmology and spectroscopic calculations. A robust iterative framework that solves the radiation intensity by treating the coupling between radiation field and matter is indeed necessary. In other words this means solving the RTE and the rate equations 'together'.

At high densities, the temperatures are also expected to be higher in SNe or in a cosmological scenario. The level populations in atoms and molecules will remain in statistical equilibrium amongst themselves. The level populations of any species (atoms or molecules) could then be calculated from equivalent Saha equation.

At very low densities, photons have a longer mean free path and the photons travel almost freely without getting absorbed or scattered due to the lack of matter particles.

Then there are the intermediate densities where matter and radiation are not strongly coupled nor completely decoupled. One needs to address the question of radiative transfer more carefully in this regime.The level populations deviate significantly from their thermal equilibrium values at these regimes. One interesting problem to look at was how hydrogen recombination would behave in this scenario. We have concluded that for SNe like steep density profile,

1)Expectantly, the ionization fraction of hydrogen is strongly dependent on the composition of the environment.In absence of metals, with a strong SNe like density profile, ionization fraction is substantially reduced if there are many angular-momentum sub-states and high shell number.

2) The 2-photon process connecting 2s and 1s level of hydrogen is effective towards recombination of hydrogen. This effect is more important in a pure hydrogen environment as compared to a metal-rich one.

3) For SNe, we believe except in early times the recombination rate is overestimated in the current literature and mentioned to be comparable to the age of the SNe. We claim that this is an over estimation of recombination time. Detailed calculations prove that recombination time is indeed much smaller than the expansion time of SNe (Type II), in a true multi-level framework. The detailed calculation also provide a fit to hydrogen lines in the observed spectra of SN 1987A. This indicates that our estimate on recombination time is indeed based on realistic values of parameters.

4)Studying hydrogen recombination in detail for SNe like steep density profiles, also opened up the great opportunity to look for information in the cosmology front by applying the same framework. The difference was density and expansion structures.There is a large portion of this problem that is yet to be answered which will be a very interesting future work to pursue. We hope with new high S/N data from Planck satellite from CMB or future satellites will be useful for this purpose.

Bibliography

Alpher, R. A., Herman, R., & Gamow, G. A. 1948, Physical Review, 74, 1198

Arnett, W. D., Bahcall, J., Kirshner, R. P., & Woosley, S. E. 1989, Ann. Rev. Astr. Ap., 27, 629

Barlow, M. J. Prospects for Studies of Stellar Evolution and Stellar Death in the JWST Era, 247–+

Baron, E., Nugent, P. E., Branch, D., Hauschildt, P. H., Turatto, M., & Cappellaro, E. 2003, ApJ, 586, 1199

Branch, D. 1987, ApJ, 320, L23

Branch, D. & Nomoto, K. 2007, Nature, 447, 393

Branch, D., Perlmutter, S., Baron, E., & Nugent, P. 2001, ArXiv Astrophysics e-prints

Carlsson, M., Rutten, R., & Shchukina, N. 1992, A&A, 253, 567

Castor, J. I. 1970, MNRAS, 149, 111

Chandrasekhar, S. 1934, MNRAS, 94, 444

Danziger, I. J., Bouchet, P., Fosbury, R. A. E., Gouiffes, C., & Lucy, L. B. 1988, in Supernova 1987A in the Large Magellanic Cloud, ed. M. Kafatos & A. G. Michalitsianos (Cambridge: Cambridge University Press), 37–50

De, S., Baron, E., & Hauschildt, P. H. 2009, MNRAS, 401, 2081

De, S., Baron, E., & Hauschildt, P. H. 2010, ArXiv e-prints

Dessart, L. & Hillier, D. J. 2005, A&A, 439, 671

Dessart, L. & Hillier, D. J. 2008, MNRAS, 383, 57

Dicke, R. H., Peebles, P. J. E., Roll, P. G., & Wilkinson, D. T. 1965, ApJ, 142, 414

Gamow, G. 1948, Nature, 162, 680

Grin, D. & Hirata, C. M. 2010, Phys Rev D, in press, astro-ph/0911.1359

Hanuschik, R. W. & Dachs, J. 1988, Astronomy and Astrophysics, 205, 135

Hauschildt, P. H. 1992, JQSRT, 47, 433

Hauschildt, P. H. & Baron, E. 1999, J. Comp. Applied Math., 109, 41

—. 2004, Mitteilungen der Mathematischen Gesellschaft in Hamburg, 24, 1

Hauser, M. HST and JWST: Present and Future, 273–+

Hillier, D. J. & Miller, D. L. 1998, ApJ, 496, 407

Höflich, P. 1988, Proceedings of the Astronomical Society of Australia, 7, 434

Höflich, P. 2003, in Astronomical Society of the Pacific Conference Series, Vol. 288, Stellar Atmosphere Modeling, ed. I. Hubeny, D. Mihalas, & K. Werner (San Franciso: ASP), 185

Howell, D. A., Conley, A., Della Valle, M., Nugent, P. E., Perlmutter, S., Marion, G. H., Krisciunas, K., Badenes, C., Mazzali, P., Aldering, G., Antilogus, P., Baron, E., Becker, A., Baltay, C., Benetti, S., Blondin, S., Branch, D., Brown, E. F., Deustua, S., Ealet, A., Ellis, R. S., Fouchez, D., Freedman, W., Gal-Yam, A., Jha, S., Kasen, D., Kessler, R., Kim, A. G., Leonard, D. C., Li, W., Livio, M., Maoz, D., Mannucci, F., Matheson, T., Neill, J. D., Nomoto, K., Panagia, N., Perrett, K., Phillips, M., Poznanski, D., Quimby, R., Rest, A., Riess, A., Sako, M., Soderberg, A. M., Strolger, L., Thomas, R., Turatto, M., van Dyk, S., & Wood-Vasey, W. M. 2009, ArXiv e-prints

Hu, W. 2003, Annals of Physics, 303, 203

—. 2008, ArXiv e-prints

Hubeny, I., Blaes, O., Krolik, J. H., & Agol, E. 2001, ApJ, 559, 680

Hummer, D. G. & Storey, P. J. 1987, MNRAS, 224, 801

Kashlinsky, A., Mather, J., & Odenwald, S. 1999, in American Astronomical Society Meeting Abstracts, Vol. 194, American Astronomical Society Meeting Abstracts, 113.02–+

Kurucz, R. L. 1995, Highlights of Astronomy, 10, 579

Mazzali, P. A., Lucy, L. B., & Butler, K. 1992, A&A, 258, 399

Menzel, D. H. & Cillié, G. G. 1937, ApJ, 85, 88

Mihalas, D. 1970, Stellar atmospheres (Series of Books in Astronomy and Astrophysics, San Francisco: Freeman, —c1970)

Mihalas, D. 1978, Stellar Atmospheres (New York: W. H. Freeman)

Olson, G. L. & Kunasz, P. B. 1987, JQSRT, 38, 325

Osterbrock, D. 1989, Astrophysics of Gaseous Nebulae and Active Galactic Nuclei (Mill Valley, CA: University Science Books)

Parthasarathy, M., Branch, D., Jeffery, D. J., & Baron, E. 2007, New Astronomy Review, 51, 524

Pastorello, A., Zampieri, L., Turatto, M., Cappellaro, E., Meikle, W. P. S., Benetti, S., Branch, D., Baron, E., Patat, F., Armstrong, M., Altavilla, G., Salvo, M., & Riello, M. 2004, MNRAS, 347, 74

Peebles, P. J. & Ratra, B. 2003, Reviews of Modern Physics, 75, 559

Peebles, P. J. E. 1968, ApJ, 153, 1

Peebles, P. J. E., Seager, S., & Hu, W. 2000, ApJ, 539, L1

Perlmutter, S. et al. 1999, ApJ, 517, 565

Petkova, M. & Springel, V. 2009, MNRAS, 396, 1383

Poznanski, D., Baron, E., Blondin, S., Bloom, J. S., D'Andrea, C., Della Valle, M., Dessart, L., ellis, R. S., Gal-Yam, A., Goobar, A., Hamuy, M., Hicken, M., Kasen, D. N., Krisciunas, K. L., Leonard, D. C., Li, W., Livio, M., Marion, H., Matheson, T., Neill, J. D., Nomoto, K., Nugent, P. E., Quimby, R., Sako, M., Sullivan, M., Thomas, R. C., Turatto, M., Van Dyk, S. D., & Wood-Vasey, W. M. 2009, in Astronomy, Vol. 2010, astro2010: The Astronomy and Astrophysics Decadal Survey, 237–+

Riess, A. et al. 1998, AJ, 116, 1009

Schmutz, W., Abbott, D. C., Russell, R. S., Hamann, W.-R., & Wessolowski, U. 1990, ApJ, 355, 255

Scott, D. & Smoot, G. 2006, ArXiv Astrophysics e-prints

Seager, S., Sasselov, D. D., & Scott, D. 2000, ApJS, 128, 407

Spergel, D. N. 2005, Physica Scripta Volume T, 117, 29

Sunyaev, R. A. & Chluba, J. 2008, in Astronomical Society of the Pacific Conference Series, Vol. 395, Frontiers of Astrophysics: A Celebration of NRAO's 50th Anniversary, ed. A. H. Bridle, J. J. Condon, & G. C. Hunt, 35–+

Sunyaev, R. A. & Chluba, J. 2009, Astronomische Nachrichten, 330, 657

Tsuruta, S. & Nomoto, K. 1988, Astrophysical Letters Communications, 27, 241

Tytler, D., O'Meara, J. M., Suzuki, N., & Lubin, D. 2000, Phys. Rep., 333, 409

Utrobin, V. P. & Chugai, N. N. 2005, Astronomy and Astrophysics, 441, 271

Williams, R. E. 1987a, ApJ, 320, L117

Williams, R. E. 1987b, in Atmospheric Diagnostics of Stellar Evolution, ed. K. Nomoto (Berlin: Springer), 118

Wong, W. Y., Seager, S., & Scott, D. 2006, MNRAS, 367, 1666

Zeldovich, Y. B., Kurt, V. G., & Syunyaev, R. A. 1969, Soviet Journal of Experimental and Theoretical Physics, 28, 146